Accounts

Molecular Simulations of Photoaddition Selectivity and Chirality in Challenging Photochemical Reactions

Kenichi Somekawa,* Yuka Odo, and Tetsuro Shimo

Department of Applied Chemistry and Chemical Engineering, Faculty of Engineering, Kagoshima University, 1-21-40 Korimoto, Kagoshima 890-0065

Received March 2, 2009; E-mail: some@apc.kagoshima-u.ac.jp

The origins of cycloaddition selectivities and chirality controls in particular and challenging photochemical reactions were examined. The profiles of the energies and stereochemical changes of the photoreactions were characterized by molecular simulations using dynamic molecular orbital methods. The photoreactions possess particular factors which are not explained by the frontier molecular orbital (FMO) theory. Particular photoreactions are examined by following the addition selectivities and two chiral controls by use of chiral hosts. (1) Species-(singlet or triplet), peri-, site-, regio-, and stereo-selectivities in the $[2+2]$cycloadditions and $[4+4]$cycloadditions of 2-pyridone (**1**). (2) Inversion of regioselectivity (hh/ht ratio) by the linkage-length in intramolecular $[2+2]$cycloadditions of α,β-unsaturated furanones **7** and by the alkene ring-size in intermolecular $[2+2]$cycloadditions of cycloalkenecarboxylates **11**–**13** with 2-cyclohexenone (**10**). (3) The occurrence of the hydrogen-shift reaction in the $[2+2]$photocycloaddition system between 4-hydoxycoumarin (**17**) and 3,4-dihydro-2*H*-pyran (**18o**). (4) Chiral control of selective $[4\pi]$-electrocyclic isomerizations of **1** to photopyridone **20** by hydrogen-bonding of chiral amide hosts **21**. The singlet excited state, **1*** was inferred to be enantiomeric conformers, $\mathbf{1^*}_{(+)}$ and $\mathbf{1^*}_{(-)}$, and the complex **1**·(*l*)-**21** proceeds to $\mathbf{1^*}_{(+)}$·(*l*)-**21**, followed by quenching to (*R*)-**20**. (5) Sensational chiral isomerization of (*Z*)-cyclooctene (**28Z**) to chiral (*E*)-cyclooctene (**29E**) by chiral benzenepolycarboxylates (**30**). **28Z** was inferred to accompany asymmetric **28Z** and the diastereomeric exciplexes **Ex1** (**28Z**·**30***) and proceeds with chiral isomerization via the one-sided rotation to **Ex2** (**29E***·**30**), followed by quenching to chiral **29E**. The molecular simulations for the photoreactions by MOPAC-PM5, (PM3 for hydrogen-bonding), UCIS (for singlets), and UB3LYP (for triplets) are found to be successful and show that the origin of the photoreaction selectivities is essentially determined by the first step (TS1) energies and the stereochemistries are dependent on the excited species presented in the Concluding Remarks. We also propose some applications of the molecular simulations.

1. Introduction

The origins of biomolecular homochirality in the sunlight biosphere and each reaction selectivity in the photoexcited surroundings[1] represent one of the most interesting and contentious issues in chemical evolution.[2] The homochirality and reaction selectivity in photochemical reactions represent key steps in organic syntheses of molecules.[3] The reaction mechanism suggested by frontier molecular orbital (FMO)[4] theory and the rules of conservation of orbital symmetry made by Nobel Laureates[5] are limited to reactions which have large orbital interactions between the frontier molecular orbitals (HOMO and/or LUMO) during the initial stages of the reactions.[6] Many types of photoreactions have been examined in the past 50 years.[1,7] However, the reaction selectivities of particularly unusual and interesting photoreactions[8–11] have been difficult to understand under the FMO rule. We have explored experimental photoadditions[12–16] and the synthetic application for HIV drug development[17] and new kinds of heterocyclic compounds[18–20] over the past 40 years. The FMO analysis of the regioselective reactions were effective, but limited by factors such as dipole–dipole interactions.[13] We recently performed molecular simulations[16,21–26] for challenging cycloadditions,[9–11] enantioselective photocyclizations mediated by chiral hosts in solution[25,27] and interesting photosensitized enantiodifferentiating isomerizations.[26–30] Herein we present the following account of the original analyses of two types of photoreactions of chirality controls[25–27,31] and photoaddition selectivity control.[16,22–24] Points (1)–(5) describe the photoaddition selectivity controls, whereas (6) and (7) cover chirality controls.

(1) Peri- and regio-selectivities in $[4+4]$photodimers **2** of singlet 2-pyridone (**1**):[24] Pyridone photochemistry has been extensively studied by the Hammond, Dilling, Kaneko, Hongo, and Sieburth groups, because of several interesting and important factors associated with the lactam photoproducts,

Published on the web December 10, 2009; doi:10.1246/bcsj.82.1447

substituent effects and clear photoexcited states.[32] The unusual preparation of anti-3,6-ht-[4 + 4]photodimer **2** was not, however, explained by MO theory.

(2) Site-, regio-, and stereoselectivities in singlet or triplet [2 + 2]photocycloadditions (for **4–6**) of 2-pyridones **1** with acrylates **3**:[24] Some groups have studied the photophysical properties and photoreactions between **1** and substituted alkenes including alkynes and maleimides.[32f] Comprehensive discussions on the species-(singlet and triplet) peri-, site-, regio-, stereo-, and substituent-selectivities have rarely been presented.[13,24,32f]

(3) Inversion of regioselectivity (hh/ht) in intramolecular [2 + 2]photocycloadditions (for **8** and **9**) of two α,β-unsaturated ω-alkenyl-furanones **7**, in which the inversion has been found to be dependent on the arm-length:[10,23] The intramolecular [2 + 2]photocycloaddition of cyclic enones possessing proper alkene side-chains is certainly one of the most applied reactions in organic systhesis.[3] Winkler et al. synthesized bioactive ingenol via the regioselective intramolecular dioxenone photocycloaddition reaction. The arm-conformation incorporated by a chlorine atom was recognized to be effective for the photoaddition.[3a] Besides our work,[23] there is no molecular orbital explanation for the unusual inversion of regioselectivity in the intramolecular photoadditions.[10,23]

(4) Inversion of regioselectivity (hh/ht) in intermolecular [2 + 2]photocycloadditions of cyclohexenones **10** with cycloalkenecarboxylates **11**, **12**, and **13**, was found to be dependent on the alkene ring-size:[11,22] Schuster has reviewed mechanistic aspects and regiochemistry in enone-alkene [2 + 2]photocycloadditions.[9] The chemistry does not follow the simple pattern from "regioselectivity inversion" data by Lange et al.[11] and particular mechanisms caused by 1,4-biradicals were suggested.[9] There are also theoretical studies of [2 + 2]photocycloadditions of acrolein to alkenes, and cyclic enone or acyclic enone to ethylene.[33] These studies did not describe the regiochemistry inversion.

(5) The occurrence of the hydrogen-shift reaction involving the photoreaction of 4-hydroxycoumarin (**17**) with 3,4-dihydro-2*H*-pyran (**18o**):[16] We have observed photocycloaddition controls by intermolecular hydrogen-bonding (H-bonding) that afford endo-[2 + 2]cycloadducts efficiently, in which there is no MO explanation.[34] Our hydrogen-shift event was inferred to be derived from an intermolecular H-bond.

(6) Chiral control of a [4π]-electrocyclic reaction (for photopyridone **20**) of **1** using H-bonding of chiral amide hosts **21**:[25,31] The photoisomerization of **1** for photopyridone **20** represents a disrotatory [4π]-electrocyclic reaction following Woodward–Hoffmann rules.[4–6] **20** is very interesting in photoreaction theory,[25] syntheses of chiral β-lactams and carbocyclic oxetanocins[10,32] and photoenergy storage by the large energy difference between **1** and **20**.[25] Bach et al. conducted enantioselective photochemical reactions based on the stoichiometric use of the chiral complexing agent possessing H-bonding ability;[27] however no MO explanation was provided. We have achieved excellent photocycloaddition by the use of intermolecular H-bonds in the solid state and have provided a molecular simulation explanation.[35] We then examined the production of our hosts and the photochemical reactions were characterized by an MO explanation.[25] [6π]-Electrocyclic photochromic reactions with chirality were reviewed in detail by Yokoyama.[3d] An MO explanation of the stereochemistry and energy is also available.

(7) Photosensitized chiral isomerization of (*Z*)-cyclooctene (**28Z**) for (*R*)-(*E*)-cyclooctene ((*R*)-**29E**) by chiral benzenepolycarboxylates **30**:[26,28–30] (Z–E)-Isomerization of cycloalkenes may be one of the most simple reactions. A recent review by Mori et al. was devoted to the photochemical isomerization of cycloalkenes, especially to the enantiodifferentiating photoisomerization in view of asymmetric photochemistry.[30] The review did not present any molecular level explanation. Our molecular simulation indicates an enantiomeric conformation of **28Z**.[26]

The molecular simulations of the whole photoreaction processes indicate that the energies and stereochemistries of the first steps essentially determine the reaction selectivities. The MO method and the level of the calculations have been presented in detail in each paper.

2. Simulation of Photocycloadditions

2.1 Direct Photodimerization of 2-Pyridone (1). 2.1.1 The Photoirradiation Result and the Analysis by a Frontier Molecular Orbital (FMO) Method: As shown in Scheme 1, direct photoirradiation of **1** in solution gives the anti-3,6-[4 + 4]cycloaddition dimer **2**, which is derived via an excited singlet state and **2** is one of the resulting adducts.[32a,32b,32f] Figure 1 shows energy levels and coefficients of the FMO in the ground state **1g** and excited single state **1s** of **1** by the PM5 level. The energy difference between the HSOMO–LUMO

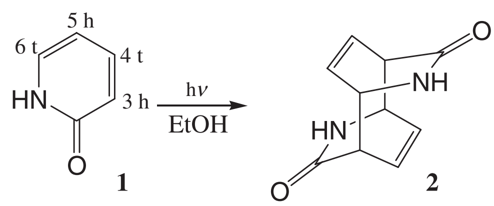

Scheme 1.

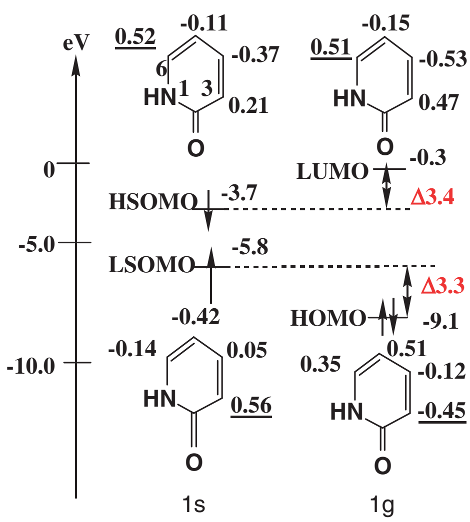

Figure 1. Energy levels and coefficients of FMO in the ground state **1g** and excited singlet state **1s** of 2-pyridone (**1**).

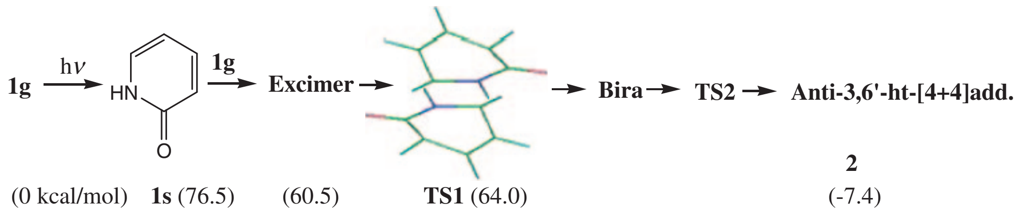

Scheme 2.

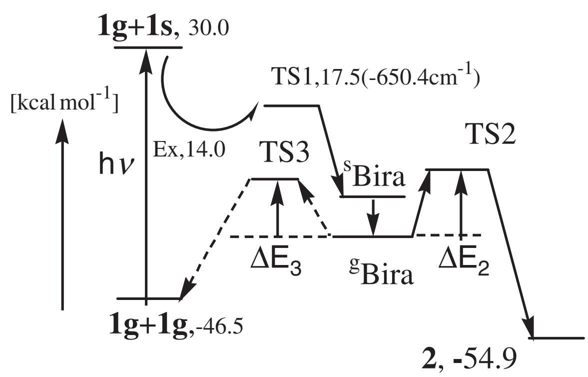

Figure 2. Photodimerization process of singlet 2-pyridone **1s**.

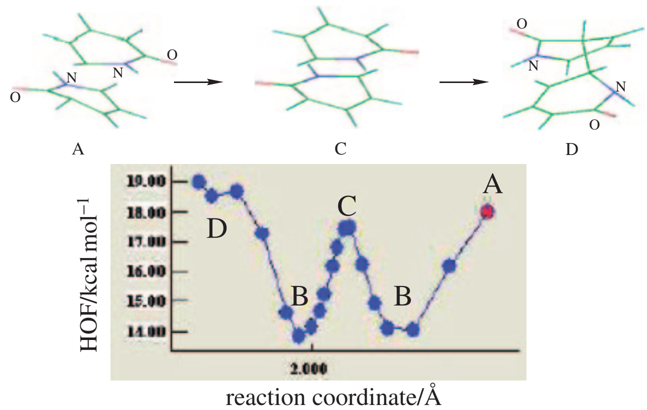

Figure 3. First transition state (TS1: C) and excimer (B) information for anti-3,6′-ht-[4 + 4]-photodimer **2**.

Table 1. Transition State Energies (TS1, TS2, and TS3) (kcal mol^{-1}) for Some Photodimerizations of 2-Pyridone (**1**)

	Addition selectivity						
	3,3′-hh		3,6′-ht		6,3′-ht		6,6′-hh
	Syn	Anti	Syn	Anti[a)]	Syn	Anti[a)]	Anti
TS1	—[b)]	26.0	19.3	**17.5**	19.3	**17.5**	26.1
TS2	—	−5.5	−13.4	−12.9	−13.3	−12.9	−5.3
ΔE_2	—	13.4	0.3	9.2	0.3	9.2	−19.7
TS3	—	−17.9	−16.1	−15.5	−16.1	−15.5	−17.9
ΔE_3	—	1.3	5.5	6.7	5.5	6.7	1.3

a) Experimental product: anti-3,6-ht-dimer. b) TS data was not obtained.

interaction and the LSOMO–HOMO interaction for the FMO analysis is negligible. The two interactions suggest the formation of a head–head (hh) or tail–tail (tt) adduct, which differs from the experimental adduct (i.e., **2**; ht adduct).[24]

2.1.2 Simulation Analysis for the Product 2 by PM5: Scheme 2 and Figure 2 show the photodimerization process of **1** to **2** by the approach between **1s** and **1g** via the first transition state (TS1), the biradical intermediate (Bira), and the second transition state (TS2). The excimer and cleavage to the reactant **1** via the third transition state (TS3) were also considered.

Figure 3 shows the first transition state (TS1: point C (17.5 kcal mol^{-1} (1 kcal mol^{-1} = 4.184 kJ mol^{-1}); −650.4 cm^{-1})) and excimer **B** (14.0 kcal mol^{-1}) information by approach of **1g** to **1s** for the anti-3,6′-ht-[4 + 4]photodimer **2**. The horizontal reaction coordinate (Å) indicates that the distance between C_3 and $C_6{}'$, and the vertical potential energies (kcal mol^{-1}) is the heat of formation (HOF) under the reaction conditions employed; in this case the PM5 method.

The TS1 ($r_{3,6'} = 2.14$ Å) is inferred as the real transition state by the frequency analysis. The calculated excimer **B** ($r_{3,6'} = 1.9$ and $r_{3',6} = 2.4$ Å) proves theoretically the excimer by our fluorescence quenching experiments.[13] TS2 and TS3 are calculated by ring-closure and cleavage of the first bond from the ground state biradical (^{g}Bira). Table 1 shows the transition state energies (TS1, TS2, and TS3) for real and postulated photodimerizations of 2-pyridone (**1**).

The TS1 (17.5 kcal mol^{-1}) of the real anti-3,6-ht **2** is lower than the other TS1 values, and supports the experimental result. The parallel anti-structures of the transition state and excimer **B** in Figure 3 suggest that the ionic interactions between the 3 and 6′ positions are more effective than orbital overlapping interactions. The higher TS2 (ring-closure) than TS3 (cleavage to the reactant) also suggests the presence of high fluorescence quenching by high **1** concentrations.[36]

2.2 Singlet and Triplet Photocycloadditions between 2-Pyridone (1) and Methyl Acrylate (3). 2.2.1 Singlet Photoreactions: The photoreactions of **1** with substituted ethylenes such as **3** have been shown to be strongly dependent on the type of substituents.[13,32f,36] Scheme 3 shows the direct reaction of **1** with **3** and the three types of products that arise from this reaction: the major endo-3,4-ht-[2 + 2]adduct **4d**; an endo-5,6-hh-[2 + 2]adduct **5d**; and a novel azocinonecar-

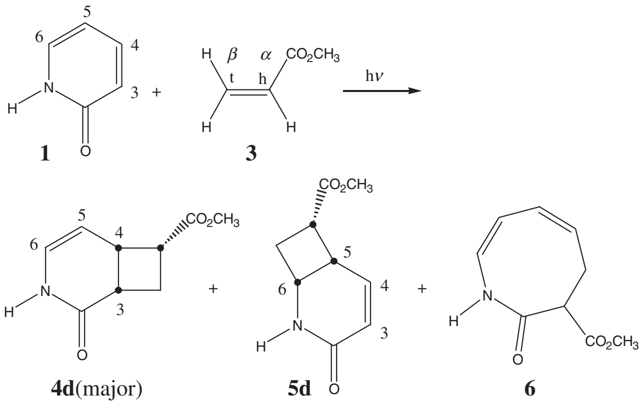

Scheme 3.

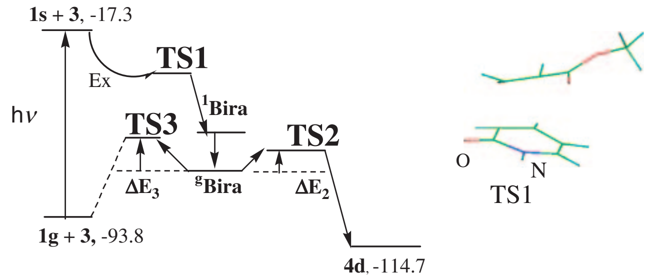

Figure 4. Singlet photoaddition process and energy diagram of **1s** with **3**.

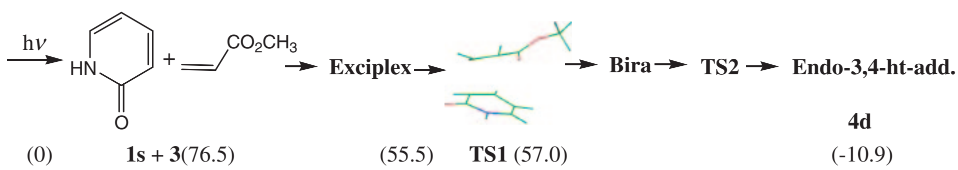

Scheme 4.

Table 2. Transition State and Biradical Intermediate Energies in the 3,4-[2 + 2]Cycloadditions between Singlet **1s** and **3**

Run	Reaction selectivity	Exp. adduct, %	HOF by PM5/kcal mol^{-1} TS1	^{1}Bira	^{g}Bira	TS2	ΔE_2	(^{g}Bira)	TS3	ΔE_3	Adduct
1	hh endo		−25.3	−53.2		concerted		reaction			−113.9
2	exo		−24.5	−52.2		concerted		reaction			−114.2
3	ht endo	**4d**, 38	−36.8	−43.5	−76.2	−74.2	2.0	(−77.9)	−68.5	9.4	−114.7
4	exo		—	−48.0	−76.7	−73.3	13.0	(−78.7)	−68.6	10.1	—

Table 3. Transition State and Biradical Intermediate Energies for the Azocinone **6** Formation from **1s** with **3**

Exp. adduct, %	HOF by PM5/kcal mol^{-1} TS1	^{1}Bira	^{g}Bira	TS2	ΔE_2	TS3	ΔE_3	**6**
6, 4	−28.6	−52.5	−84.9	−72.9	12.2	−51.4	33.9	−99.5

boxylate **6**.[36] The major **4d** preparation and the ht regioselectivity are not easily explained by FMO. Formation of **5d** (one hh adduct) can be explained by FMO (a HSOMO–LUMO interaction). The excited singlet reaction mechanism was inferred by fluorescence quenching of **1** by **3**. The whole process and energy diagram were also inferred (Scheme 4 and Figure 4) by the TS analysis and the approach of **1s** with **3**.[24]

Table 2 shows the TS and biradical intermediate energies in the 3,4-[2 + 2]cycloadditions between **1s** and **3** by PM5. The major preparation of **4d** (endo-ht-[2 + 2]adduct) is inferred from the lowest TS1 energy, whose parallel structure (Figure 4) suggests a concerted reaction by π–π^* interactions.

Figure 5 shows the proposed reaction process for a novel azocinone **6** via an excited biradical **^{1}Bira** involving a singlet reaction of **1s** with **3**. Table 3 shows the intermediates and the energies for azocinone **6** from **1s** with **3**. The reaction mechanism for **6** proposed in a previous paper from our group[24] is corrected and presented in Figure 5 and Table 3.

2.2.2 Triplet Photoreactions: Scheme 5 shows triplet reactions of **1** with **3** in the presence of benzophenone, in which an exo-5,6-hh-[2 + 2]adduct **5x** is a major product. The exo-5,6-hh regioselectivity can be easily explained by the triplet HSOMO–LUMO interaction.[13] The process and energies are shown in Scheme 6, Figure 6, Figure 7, and Table 4. In the

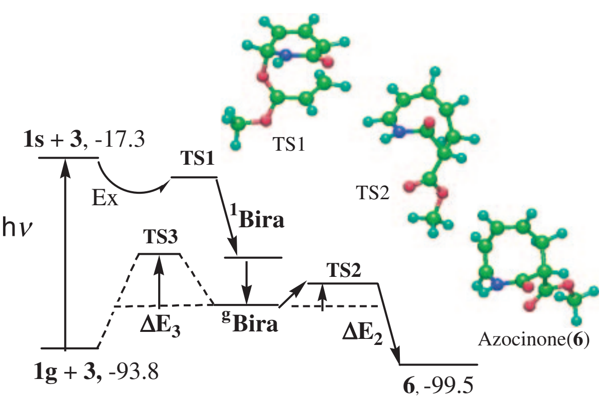

Figure 5. Energy diagram for azocinone **6** formation from **1s** with **3**.

TS1 structure (**B** in Figure 7) for **5x**, the position between **1t** and **3** is slanting ($r_{1(6)\text{–}3(\beta)} = 2.15$ Å). The energies and structures in the process are characteristic of triplet reactions.[13,24] The TS1 (-42.2 kcal mol^{-1}) for **5x** by PM5 is 1.6 kcal mol^{-1} higher than the TS1 for **4x**. The calculated value at the UCIS/PM5 level is consistent with the experimental **5x**/**4x** ratio.[24]

2.3 Origin of Regioselectivity in the Intramolecular [2 + 2]Photocycloadditions of α,β-Unsaturated Furanones 7 to the Terminal Alkene. 2.3.1 Inversion of the Regioselectivity in the Intramolecular [2 + 2]Cycloadditions:[10] Many synthetic uses of intramolecular [2 + 2]photocycloadditions rely on the regio- and stereo-selectivity of the products.[3] As shown in Scheme 7, this selectivity is dependent on the length of the linker between the active parts. Namely, the head–tail (ht) regioselectivity was exclusively produced through a one-carbon atom connection, whereas it was completely inverted when the connection involved two-carbon atoms. Bach and co-workers attributed this outcome to the triplet reaction.[10]

2.3.2 MO Analysis of the Regioselectivity in the Intramolecular [2 + 2]Photocycloadditions of 7:[23] Photocycloadditions of cyclic enones with alkenes normally afford cyclobutane rings from the enone triplet states.[9,33] We studied courses of additions of the triplet intramolecular photoadditions by considering two-step reactions via the formation of biradical intermediates. We have successfully used the transition state analysis to characterize the regio- and stereo-selectivities of different photoadditions and Diels–Alder reactions.[21–24] Following the triplet excitation of furanones, the enone parts underwent major changes during the computation process (Figure 8). The most stable conformers as the two triplets **7at** and **7bt** are the conformers with the alkene moiety oriented away from the enone rings. The preferred cycloadducts which are introduced from the orbital interaction by FMO are ht in both reactions. The calculations are not consistent with the experimental results. The possible pathway of the intramolecular photocycloadditions of **7a** and **7b** are presented in Scheme 8 and Figure 9. The analysis of the singlet process

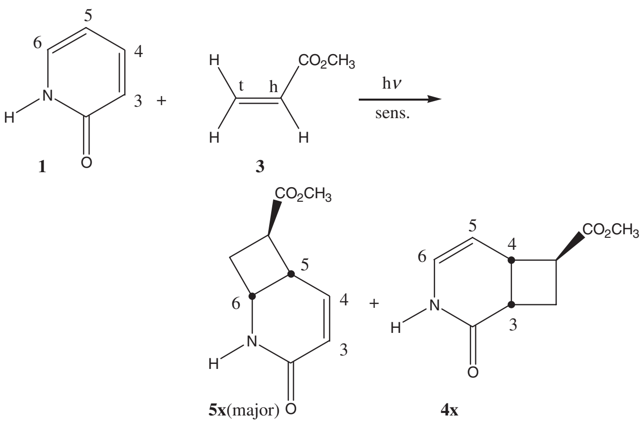

Scheme 5.

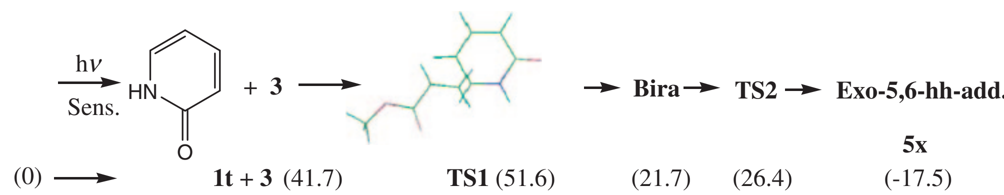

Scheme 6.

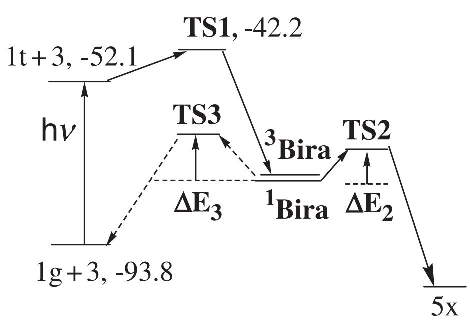

Figure 6. Photoaddition process and energy diagram of **1t** with **3**.

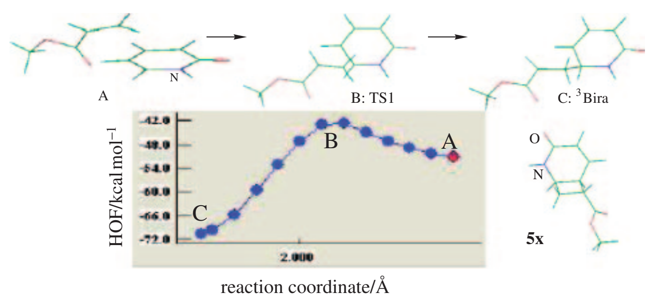

Figure 7. First transition state (TS1: B) information for exo-5,6-hh-[2 + 2]-adduct **5x** from triplet **1t** with **3**.

Table 4. Transition State Energies (TS1, TS2, and TS3) for 5,6-Cycloadditions **5x** of Triplet **1t** with **3**

Run	Reaction selectivity		Exp. adduct, %	HOF by PM5/kcal mol^{-1}							
				TS1[a]	^{3}Bira	^{1}Bira	TS2	ΔE_2	TS3	ΔE_3	Adduct
1	hh	endo		−41.7	−71.0	−72.1	−67.4	4.7	−66.1	6.0	−110.4
2		exo	**5x**, 23	−42.2	−70.5	−71.1	−68.4	2.7	−65.1	6.0	−111.3
3	ht	endo		−38.1	−73.2	−74.0	−71.4	2.6	−68.8	5.2	−111.4
4		exo		−38.5	−72.9	−74.0	−71.5	2.5	−68.9	5.1	−111.1

a) HOF (**1t** + **3**) is -52.1 kcal mol^{-1}. ΔE_1 can be calculated using each HOF of TS1.

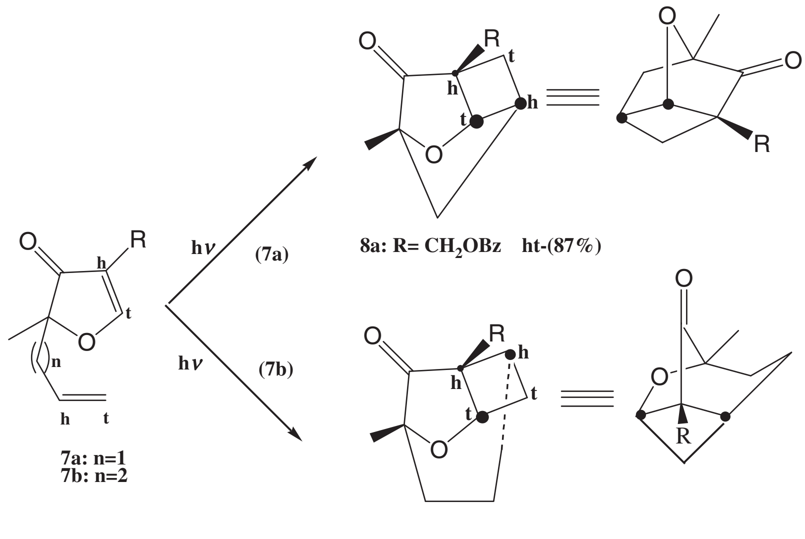

9b: R= CH$_2$OBz hh-(92%)

Scheme 7.

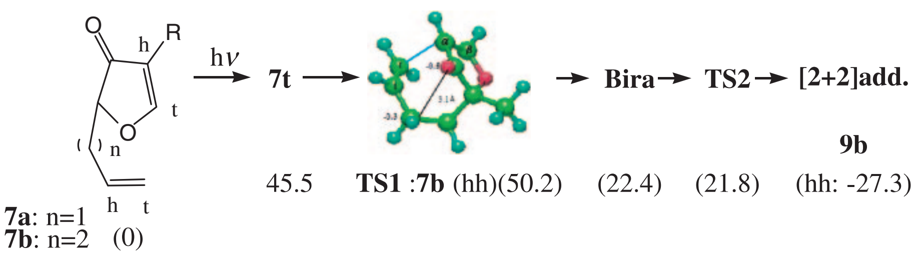

Scheme 8.

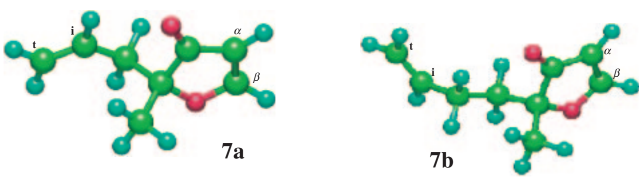

	7a		7b
$E^1{}_T$ =	**45.6**	$E^1{}_T$ =	**45.5**
$E^1{}_S$ =	**87.9**	$E^1{}_S$ =	**90.0**
$E^1{}_T$ =	66.1	$E^1{}_T$ =	66.1
$E^1{}_S$ =	*77.9*	$E^1{}_S$ =	*78.0*

Figure 8. The triplet structures of **7a** and **7b**, and the triplet ($\mathbf{E^1{}_T}$) and singlet ($\mathbf{E^1{}_S}$) energies relative to the ground state, calculated at PM5 (**Bold**) and optimized B3LYP/6-31G levels. Singlet (*italic*) state energy is calculated at CIS/6-31+G(d) level.

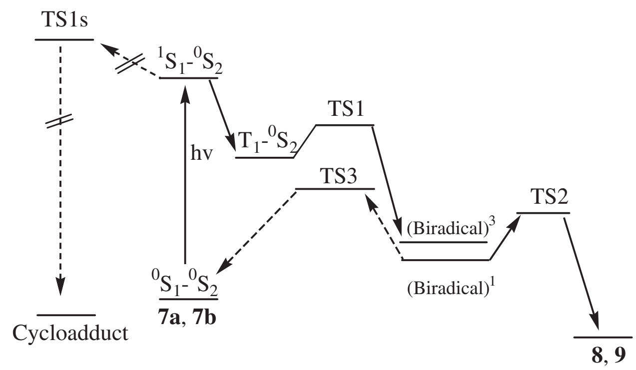

Figure 9. Estimated potential energy surface of the photoreactions produced from PM5.

between $^1S_1$ and $^0S_2$ showed cleavage of the furanone ring to give a small amount of the product. This calculation was different from the experimental results. The analysis of the triplet route between T_1 and $^0S_2$ by both PM5 and UCIS/6-31+G(d)//PM5 showed that the lowest state is the π–π^* triplet. The computed relative energies ($E_{\rm rel}$) of the potential energy surfaces (PES) in the reaction process were calculated. Table 5 shows the whole energies of the PES relative to the triplet reactions of **7a** and **7b**, in which biradical intermediates are included. Tables 6 and 7 show the first transition state energies ($E_{\rm TS1}$) for the regioselective photoadditions and the (hh–ht) energy differences of the rate-determining process for the hh- or ht-additions.

The calculated TS1 heights are almost in accordance with the product distribution. Namely, $E_{\rm TS1}$ of the major products, which are ht in **7a** and hh in **7b**, are lower than those of the minor products.

In an effort to explain the energies of the TS1, the main geometric parameters of the TS1 in **7a** and **7b** photoreactions in Figure 10 are presented. The TS1 distances that correspond to the major selectivities are shorter (2.15 Å) than those that correspond to the minor selectivities (2.16–2.19 Å). In addition,

Table 5. Energies Relative to the Triplet State Computed at PM5 Level (Bold) and at UHF/6-31+G(d)//PM5 Level

Reaction	Ground $^0S_1$–$^0S_2$	Triplet T_1–$^0S_2$	Relative energies (E_{rel})/kcal mol^{-1}				
			TS1	Biradical[1]	TS3	TS2	Cycloadduct
7a (ht: 87%)							
hh			19.8	−28.8	21.1	2.1	−46.6
	−54.9	0.0	**11.7**	**−28.0**	**−13.8**	**−22.4**	**−51.2**
	−45.6	**0.0**[a)]					
ht			13.7	−17.2	22.5	11.7	−52.8
			2.8	**−33.3**	**−13.2**	**−28.5**	**−55.9**
7b (hh: 92%)							
hh			10.5	−29.3	0.6	1.3	−55.0
	−54.8	0.0	**4.7**	**−31.3**	**−22.6**	**−29.7**	**−70.8**
	−45.5	**0.0**[b)]					
ht			26.5	−8.5	21.2	21.9	−58.2
			4.3	**−33.1**	**−21.2**	**−33.7**	**−72.8**

a) Heat of formation (HOF): −6.5 kcal mol^{-1}. b) Heat of formation (HOF): −10.7 kcal mol^{-1}.

Table 6. First Transition State Energies (E_{TS1}) for the Intramolecular [2 + 2]Photoadditions of **7a** and **7b**

Reaction/exp.	$\Delta E_{TS} = [E_{TS(hh)} - E_{TS(ht)}]$/au		
	UHF/6-31+G(d)//PM5	B3LYP/6-31G//PM5	B3LYP/6-31G[a)]
7a (ht: 87%)			
C_α–C_t (ht)	−458.352493	−461.007975	−461.023745
C_β–C_t (hh)	−458.342789	−461.002739	
7b (hh: 92%)			
C_α–C_t (ht)	−497.364201	−500.298190	−500.320035
C_β–C_t (hh)	−497.389722	−500.317378	−500.330901

a) Optimized geometry at B3LYP level.

Table 7. The (hh–ht) TS1 Energy Differences for the Intramolecular [2 + 2]Photoadditions of **7a** and **7b**

Reaction/exp.	ΔE_{TS} (exp)/kcal mol^{-1}	$\Delta E_{TS} = [E_{TS(hh)} - E_{TS(ht)}]$/kcal mol^{-1}		
		B3LYP/6-31G//PM5	B3LYP/6-31G[a)]	UHF/6-31+G(d)//PM5
7a (ht: 87%)	$\geqq$1.2[b)]	3.3	5.4	6.1[c)]
7b (hh: 92%)	$\leqq$−1.3	−12.0	−6.8	−16.0

a) Optimized geometry on the 6-31G basis set. b) $\ln \mathrm{hh/ht} \fallingdotseq -\Delta E/RT$ (at 298 K). c) The energy was converted to kcal mol^{-1}, for example: $\Delta E_{TS(hh\text{–}ht)} = -458.342788 - (-458.352493) = 0.0097$ (au) = 6.1 kcal mol^{-1}.

the former also have larger angles (C = 113°) and smaller dihedral angles ($|\tau| = 69°$). These features imply that there are geometric differences between the lower and higher TS1 energies that lead to these specific regioselectivities.

Our investigation of the intramolecular photoadditions extends to cover the stability of the biradical intermediate and its relationship with the regioselectivity preference. Gleiter et al. stated that the photochemical regioselectivity preference is regulated by the "rule of five" or the initial formation of the five-member ring intermediates.[37] Four routes of our additions are possible for each reaction. These are $C_t + C_\alpha$, $C_t + C_\beta$, $C_i + C_\alpha$, and $C_i + C_\beta$. These additions yield four different biradical intermediates that are illustrated in Scheme 9.

The biradical energies for the additions calculated at B3LYP/6-31G//PM5 and UHF/6-31+G(d)//PM5 levels showed that the C_β–C_t addition biradical (hh attach) in each reaction is the most stable.[23] A five-member ring can also be formed from the C_β–C_i attachment in **7a**. The five-membered ring is not appropriate for ring closure. The ht adduct from **7a** was formed from the C_α–C_t biradical, which is not in accord with the "rule of five" for simple reactions. Consequently, the reaction mechanism is shown in Figure 11. The product regioselectivity is dependent on the TS1 energy, but not on the FMO interactions, biradical stability, "rule of five" and the TS2 energy.

2.4 Origin of Regioselectivity Inversion in [2 + 2]Photocycloadditions of 2-Cyclohexenone 10 with Cycloalkenecarboxylates 11–13. 2.4.1 Inversion of the Regioselectivity in the Three [2 + 2]Photocycloadditions:[11] Intermolecular photocycloadditions of α,β-unsaturated carbonyl compounds with alkenes are among the most widely used processes in synthetic organic chemistry.[3] The [2 + 2]photocycloadditions of the enones were normally derived from the triplet states and FMO theory showed that the regiochemistry, i.e., hh/ht ratio of the typical reactions, was mainly dependent on the electric properties of the alkenes and the biradical intermediate properties.[6,9,13,16] Scheme 10 shows interesting experimental data of [2 + 2]photocycloadditions of cyclohexenone **10** with three cycloalkenes **11–13**, to give [2 + 2]cycloadducts **14h**, **15h** + **15t**, and **16t** (+**16h**).[11] The hh/ht regioselectivity significantly inverts with increments in the ring-size from four to six. This significant result was pointed out by Schuster in 1993 and 2003.[9] However, no attempts have been made to identify the root of the regioselectivity change and the cause of this regioselectivity is still of significant interest. FMO analysis has predicted that the hh adducts are the main products. The smaller ring-size has the marked tendency to lead to the hh adduct because of the large coefficient value at the C–β position (**11** > **12** > **13**).[22]

2.4.2 Origin Analysis of the Regioselectivity Inversion by Molecular Simulation:[22] The whole photocycloaddition pathway is presented in Scheme 11 and Figure 12. **10** is initially excited by UV irradiation from the ground state ($^0S_{10}$) to the triplet state ($^1T_{10}$) via the singlet excited state ($^1S_{10}$) and reacts with ground states ($^0S_{11}$, $^0S_{12}$, and $^0S_{13}$). Passing the first transition state (TS1), a singlet biradical intermediate (Bira),

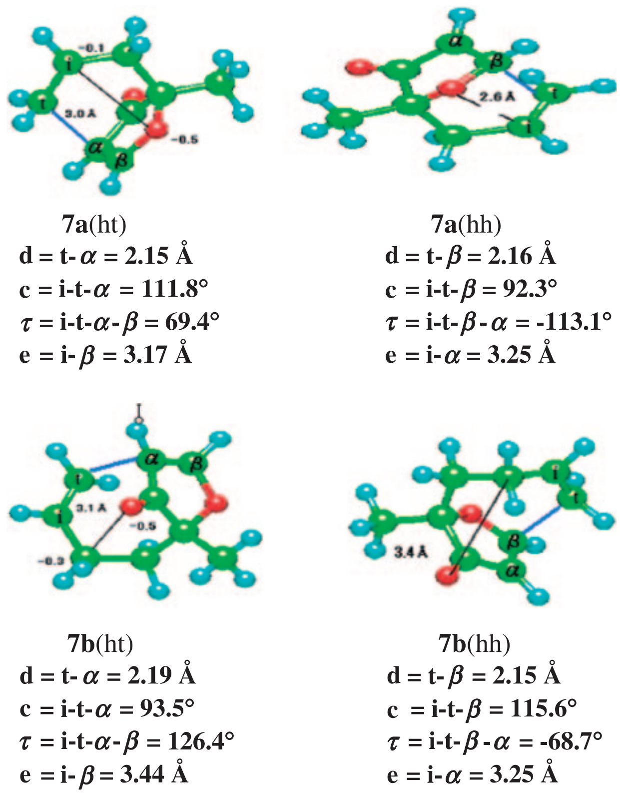

Figure 10. Transition state structures for **7a** and **7b** reactions. Charges of atoms that are expected to be repulsed are shown. **d, c**, τ, and **e** stand for distance, angle, dihedral angle, and distances prior to second bond formation consequently. Blue (thick) line stands for TS distances.

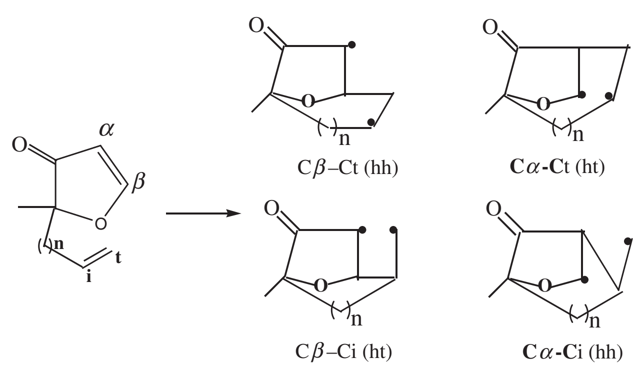

Scheme 9.

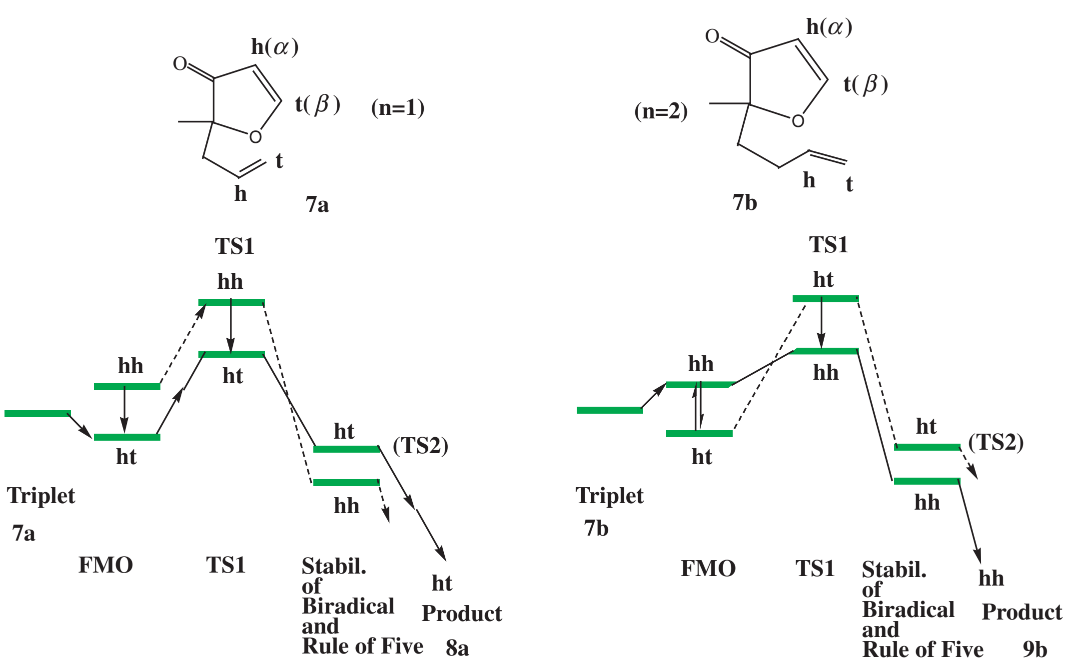

Figure 11. Photoreaction profiles and mechanism by the energy analysis.

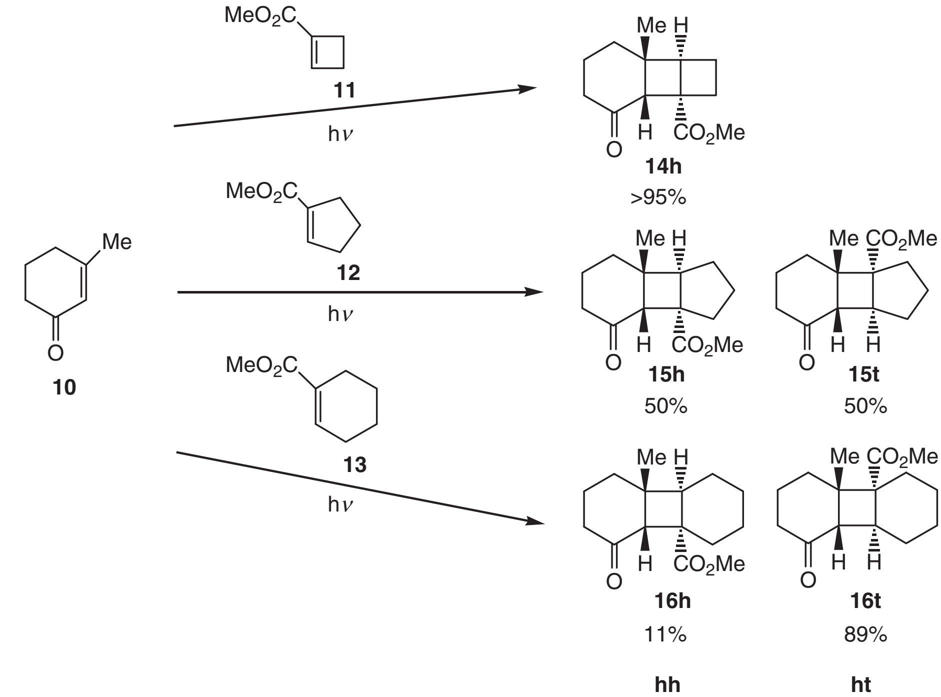

Scheme 10.

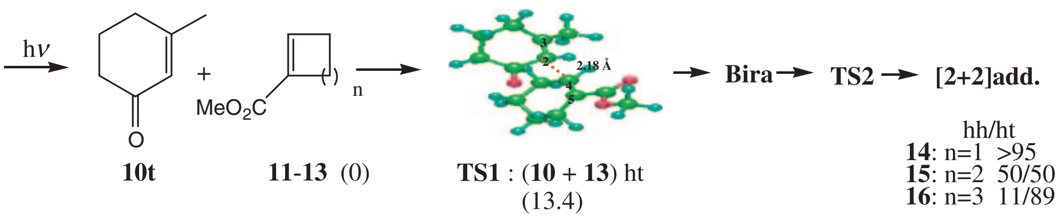

Scheme 11.

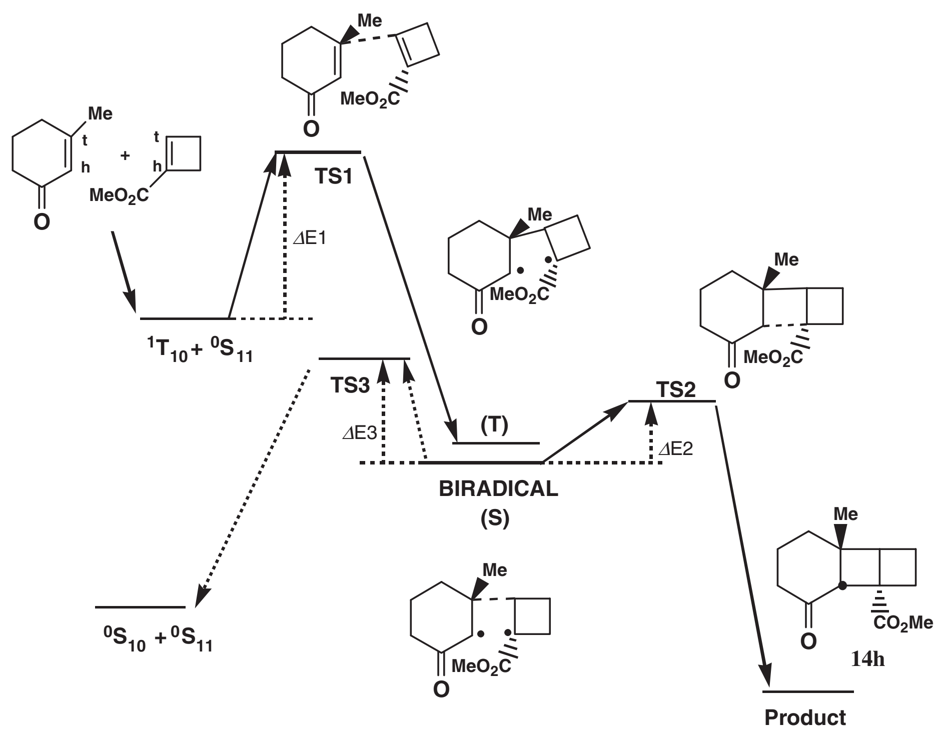

Figure 12. The triplet photocycloaddition pathway via the biradical intermediate.

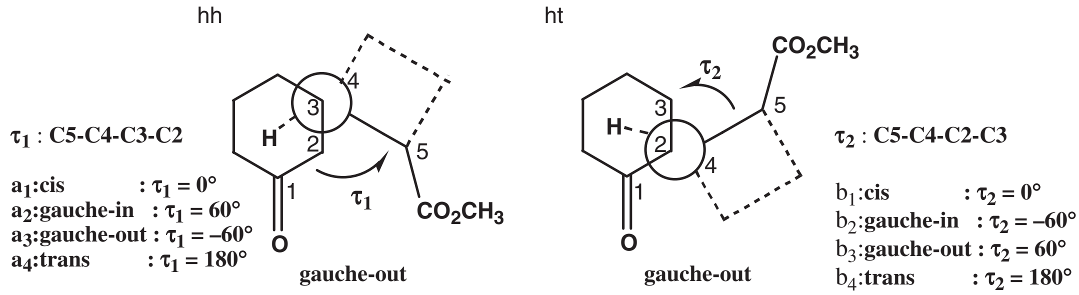

Figure 13. Four initial conditions at the starting point. Dihedral angles τ = cis, gauche-in, gauche-out, trans, for head-to-head and head-to-tail.

Table 8. The Lower Energy Barriers and the Dihedral Angles of TS1 on Regioselective Photoadditions

			Methods and energy barrier (ΔE_{act} $^{a)}$)/kcal mol^{-1}			τ/°
			PM5	B3LYP/6-31G//PM5	B3LYP/6-31+G(d)//PM5	
10 + 11	hh	a_1	11.7	1.8$^{b)}$	2.8	32.6
	ht	b_3	10.6	5.7	8.5	171.7
10 + 12	hh	a_2	13.6	9.7	6.9	169.3
	ht	b_4	11.4	6.6	5.4	−172.5
10 + 13	hh	a_1	16.6	14.2	9.7	64.0
	ht	b_1	13.4	10.4	6.8	172.4

a) $\Delta E_{act} = E(2a_1) - E(^1T_1 + {}^0S_2)$. b) 1.8 kcal mol^{-1} = −731.503206 au − {−347.775986 au + (−383.730141 au)} = 0.023 au.

and the second transition state (TS2), products **14–16** are afforded yet compete with the return to compounds **10** and **11–13** via TS3.

Figure 13 shows the initial conditions for the TS analysis, namely four initial conditions of dihedral angles for TS1: τ = cis, gauche-in, gauche-out, and trans, for the hh (a_1–a_4) and ht (b_1–b_4) regioselectivity analysis. Particular initial conditions gave identical TS1 results. Table 8 shows the lower TS1 energy barriers (ΔE_{act}) and the dihedral angles (τ) at the PM5 level and B3LYP//PM5 level for each hh and ht reaction product of **14h**, **14t**, **15h**, **15t**, **16h**, and **16t** between **10** and **11–13**. Figure 14 shows the hh and ht geometries and dihedral angles. The $C_{3(\mathbf{10})}$–$C_{2(\mathbf{11–13})}$ (for hh adducts), or $C_{2(\mathbf{10})}$–$C_{2(\mathbf{11–13})}$ (for ht adducts) distances of 2.15–2.20 Å are reasonable.

Table 9 shows the energy difference ($\Delta\Delta E$) between the lower hh-TS intermediate and the lower ht-TS intermediate on **10** + **11**, **10** + **12**, and **10** + **13** reactions by the following equation.

$$-\Delta\Delta E = -\{\Delta E(\mathrm{hh}) - \Delta E(\mathrm{ht})\} \tag{1}$$

The PM5 calculation shows that all of the reactions prefer the ht adducts because the TS1 energy of the ht adducts is smaller than that of the hh adducts in the calculation. The energy differences gradually diminish following the increase in the ring-size. Therefore, the tendency for the larger ring to produce the ht adduct is observed. If the observational errors of $-\Delta\Delta E$ are ca. 2.2 kcal mol^{-1}, the corrected values of $-\Delta\Delta E$ are 1.1, −0.0, and −1.1 kcal mol^{-1} for the **10** + **11**, **10** + **12**, and **10** + **13** reactions presented in Table 9. Consequently, the calculations correspond to the experimental results. The single-point-energy calculations at the B3LYP levels from the PM5 geometries gave energy values (3.8 and −2.9 kcal mol^{-1}) that closely matched the experimental results (1.7 and −1.2 kcal mol^{-1}) as shown in Table 9 (and Table 8). These results suggest that the TS1 surface energy of the geometry governs the regioselectivity of hh/ht and is dependent on the ring-size of the cyclic alkenes.

We also simulated TS2 of a few kcal mol^{-1} and TS3 of about 10–18 kcal mol^{-1} and found that the second-step reactions forming cyclobutanes may occur as soon as the biradical intermediates are formed.[22]

2.4.3 Deformation Energy Analysis:[22] The TS1 energies were partitioned into two deformation energies (E_{df}) and the interaction energy (E_{int}), which have been effective for the analysis of face-selectivity in the thermal cycloadditions.[21,38] The E_{df} is the energy required to change the reactants' geometry into the transition state geometry. The TS energy differences (ΔE_{act}) are partitioned as follows:

$$\Delta E_{act} = \Delta E_{df}\text{-enone} + \Delta E_{df}\text{-alkene} + \Delta E_{int} \tag{2}$$

The two E_{df} values are calculated by the following equations:

$$\Delta E_{df}\text{-enone} = \Delta E_{TS}\text{-enone} + E\text{-enone} \tag{3}$$

$$\Delta E_{df}\text{-alkene} = \Delta E_{TS}\text{-alkene} + E\text{-alkene} \tag{4}$$

E_{TS}-enone and E_{TS}-alkene are the heat of formation (HOF) of the triplet enone and the ground state alkene at the TS state, respectively. E-enone and E-alkene are the HOF of $^1\mathbf{T}_{\mathbf{10}}$ and $^0\mathbf{S}_{\mathbf{11–13}}$, respectively. E_{int} values are calculated from eqs 3, 4, and 2, and a positive value indicates some repulsion, which may come from the triplet reactions. These deformation energies were found to be dependent on the TS conformations and are shown in Figure 15.[22b] Increases in the deformation energies were dependent on the increment of the alkenes' ring-size and relatively on the hh conformation. Such repulsions

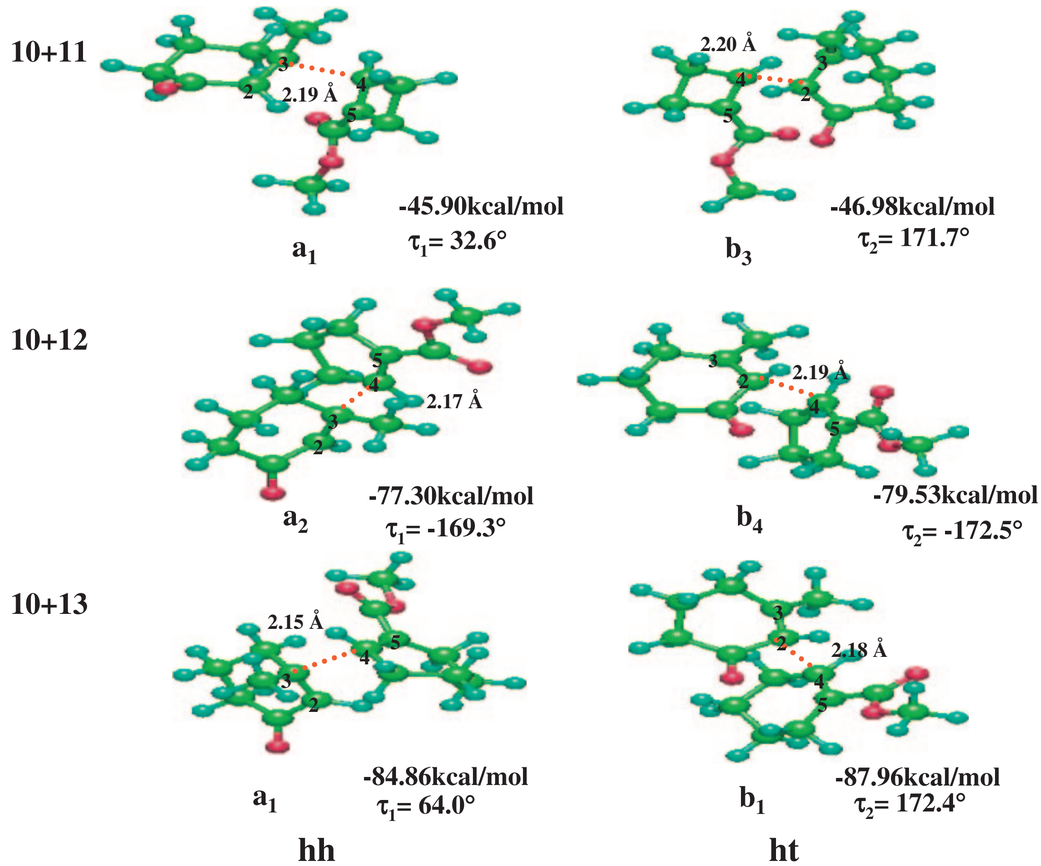

Figure 14. Transition state (TS1) geometries for the first step leading to biradical intermediates at the [2 + 2]photocycloadditions by the PM5 calculation. TS distances are in Å, dihedral angles (τ) are in degrees.

Table 9. The Energy Difference between the Lower TS1 of hh and That of ht on Photoreactions

	$-\Delta\Delta E = -\{\Delta E(\text{hh}) - \Delta E(\text{ht})\}/\text{kcal mol}^{-1}$			
	PM5		B3LYP/6-31+G(d)//PM5[b)]	Experiment[c)]
	Calculation	Corrected value[a)]	Calculation	
10 + 11	−1.1	1.1	3.8	1.7
10 + 12	−2.2	0.0	−2.3	0.0
10 + 13	−3.3	−1.1	−2.9	−1.2

a) The calculation value plus 2.2 kcal mol^{-1}. b) Single-point energy. c) ln hh/ht ≒ $-\Delta\Delta E/RT$ (at 298 K).

may electrically arise from the approach between C=O on **10** and the larger carboxylate on **13** for the hh adduct. Such repulsion gives rise to the ht adduct.

3. Origin of the Occurrence of the Hydrogen-Shift Reaction at the [2 + 2]Photocycloaddition System of 4-Hydroxycoumarin (17)

3.1 Formation of 4-Hydroxy-3-(oxan-3-yl)coumarin (19o) from Photoreaction of 17. Photochemistry of coumarin[39–44] and the basic 2-pyrones[13,15,19,20,45] has provided subjects of synthetic and mechanistic interest. We developed some interesting subjects, such as the origin of analysis of many species- and regioselective [2 + 2]cycloadditions,[13,15,19,35] ring-conversion by cleavage of cyclobutane rings[45] and the synthesis of macrocycles by double [2 + 2]cycloadditions.[20] There have been no investigations by MO analysis of photochemistry between coumarins and alkenes. We report two types of photoadditions of **17** with alkenes.[16,40] An acetonitrile solution of **17** with 3,4-dihydro-2*H*-pyran (**18o**) in the presence of benzophenone was photoirradiated to give 4-hydroxy-3-(oxan-3-yl)-coumarin (**19o**) after column-chromatography in 50% yield. The structure was confirmed by X-ray crystallographic analysis as shown in Figure 16. Since the expected [2 + 2]photoadduct $\mathbf{19_A}$ was not detected, it was inferred that the product **19o** was formed via a triplet of **17**. The mechanism of the photoreaction involved a process via a biradical **A** and a hydrogen-shift (H-shift) as shown in Schemes 12 and 13. Haywood et al. reported that photoreaction of **17** with cyclohexene (**18c**) gave a [2 + 2]cycloadduct **19c**, similar to $\mathbf{19_A}$, as shown in Scheme 14.[40] There was no explanation of the hydrogen-shift mechanism for **19o** in the same photoaddition system.

3.2 Molecular Orbital (MO) Analysis of the Hydrogen-Shift Process of the Photoaddition between Triplet 17 and 18o. The formation of **19o** is explained reasonably by

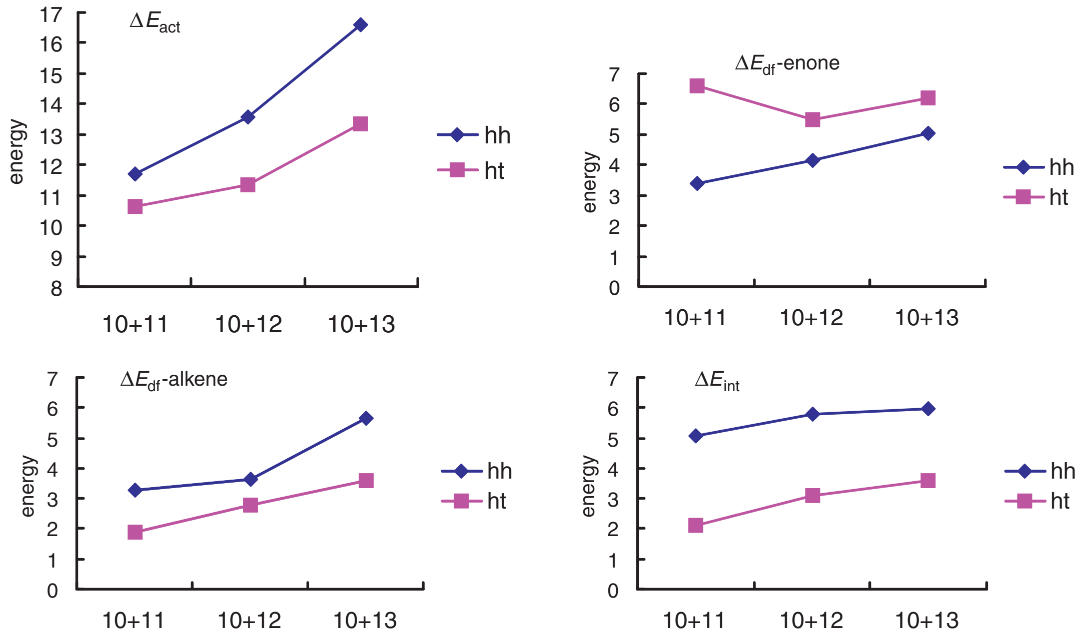

Figure 15. Relative comparison of the energy change following to the increment of the ring-size, from four to six, cycloalkene-carboxylate (**10** + **11**, **10** + **12**, and **10** + **13**). Activation energies (ΔE_{act}), deformation energies (ΔE_{df}-enone and ΔE_{df}-alkene) of enones and alkenes, and interaction energies (ΔE_{int}).

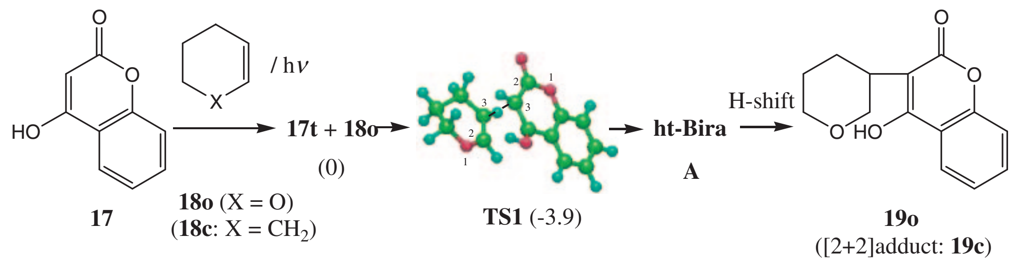

Scheme 12.

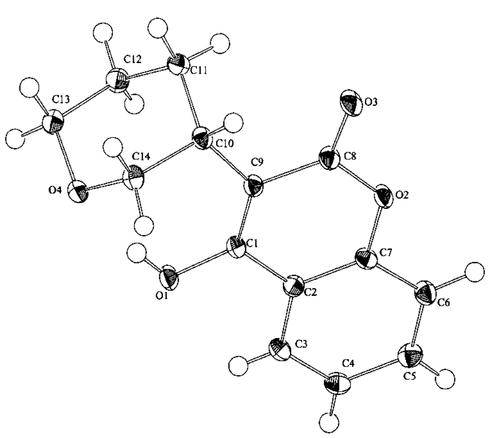

Figure 16. ORTEP drawing of compound **19o**.

consideration of a triplet photoreaction mechanism between 2-pyrone and an alkene[15] by way of a biradical intermediate **A** followed by a hydrogen shift and successive keto–enol isomerization. The inferred presence of **A** instead of **B**, **C**, and **D** in Scheme 15 also suggests that the first step addition between triplet **17** and **18o** is a head-tail (ht) addition. Such an addition orientation can be explained by the LSOMO–HOMO interaction of the narrow energy-gap and larger coefficients. The preference of the ht addition between triplet **17** (HOF: $-35.6\,\mathrm{kcal\,mol^{-1}}$) and **18o** (HOF: $-37.5\,\mathrm{kcal\,mol^{-1}}$) and the pathway were confirmed by PM5-TS analysis of the photoreactions.[16] Figure 17 shows the first-step TS structures and the energies (**AA** and **CC**) for A and C (hh radical). The TS energy of **AA** is lower than that of **CC**, and the structure of the biradical **A** has conformations whose 4-OH of **17** are close to 2-C of **18o** ($r_{OH–C} = 3.20$ Å). Such a conformation is caused by a OH/O hydrogen bonding between the 4-OH and the pyran oxygen ($r_{OH–C} = 2.80$ Å). As shown in Scheme 7, the hydrogen transfer is then inferred to occur easily. The H-bonding effect can also be inferred from our following TS analysis of the photocycloaddition between the triplet **17** and cyclohexene (**18c**). The TS energy ($-43.2\,\mathrm{kcal\,mol^{-1}}$: structure **E** in Figure 18) from the same initial geometry was a local minimum and higher than the true TS energy ($-48.2\,\mathrm{kcal\,mol^{-1}}$: structure **F** in Figure 18), and the distances between the 2-C of **18c** and 4-OH of **17** in the structures of **E** and **F** were not close because no H-bonds existed and the repulsion by 3-CH_2 of **18c** was observed.

In conclusion, the formation of product **19o** is evidence of a regioselective photoreaction pathway and the direction is suggested to be controlled by intermolecular H-bonding at the TS conditions.

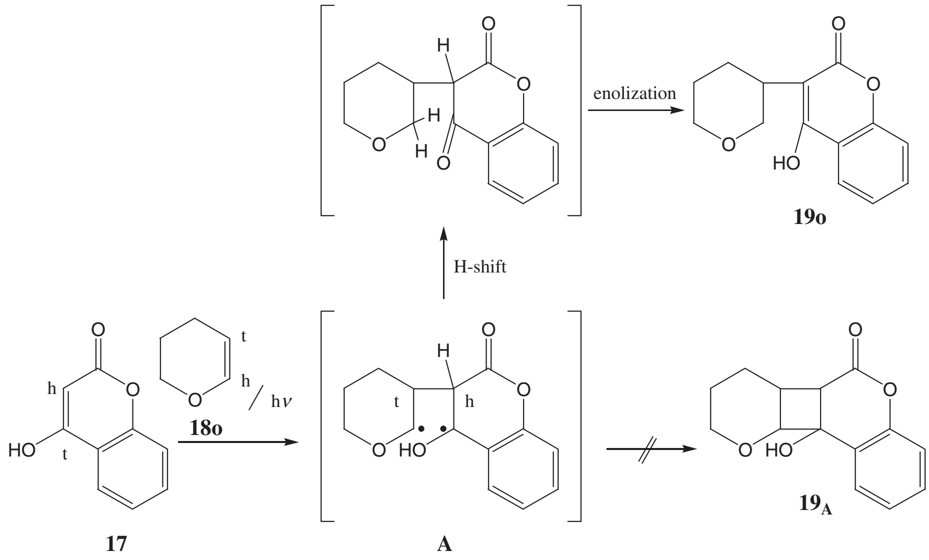

Scheme 13.

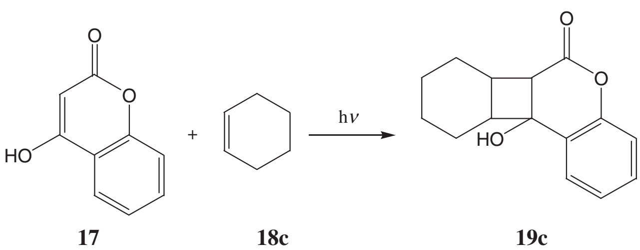

Scheme 14.

4. MO Evaluation of Enantioselective Control in Photovalence-Isomerization by Chiral Amide Hosts

4.1 Enantioselective Control in Photoisomerization of 2-Pyridone (1) to the Valence Isomer 20 Using Chiral Amide Hosts 21 and 22. We have studied how to control products and the stereochemistry of photochemical reactions.[13,26] Bach et al. reported excellent chiral control of photochemical valence-isomerization and cycloadditions of **1** and 2-quinolones by use of the H-bonding ability of a chiral host possessing Kemp's imide.[27] Preparation of the chiral host;

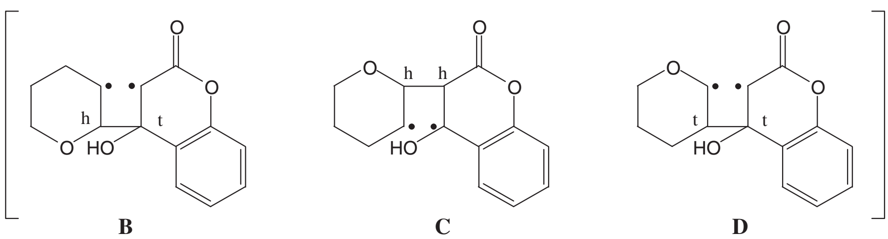

Scheme 15.

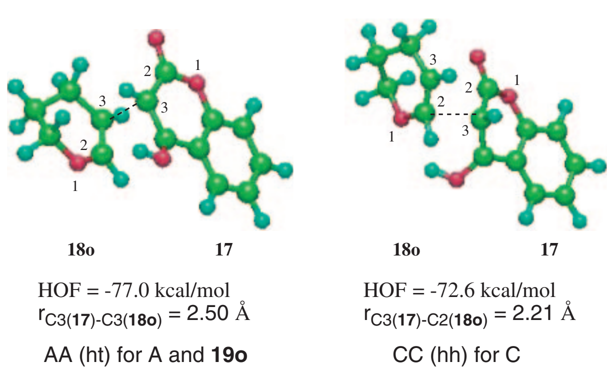

Figure 17. First-step transition state structures and energies of (triplet **17** + **18o**) photoaddition by MOPAC-PM5 method.

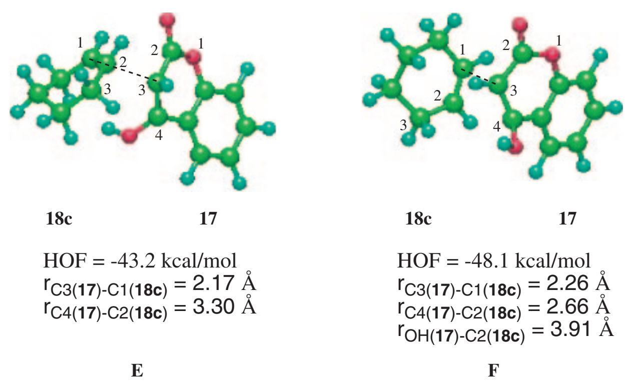

Figure 18. First-step transition state structures and energies of (triplet **17** + **18c**) photoaddition by MOPAC-PM5 method.

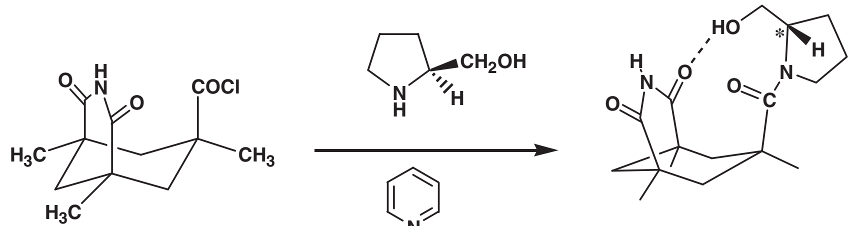

Kemp's imide chloride **imide amide 21 (69%)**

Scheme 16.

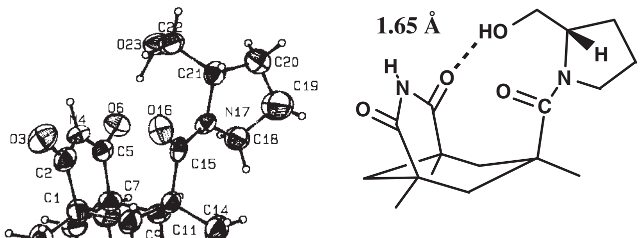

imide amide (*l*)-21
(mp: 237-239°C)

Figure 19. ORTEP drawing of imide-amide (*l*)-**21**: the dashed line indicates a hydrogen bond.

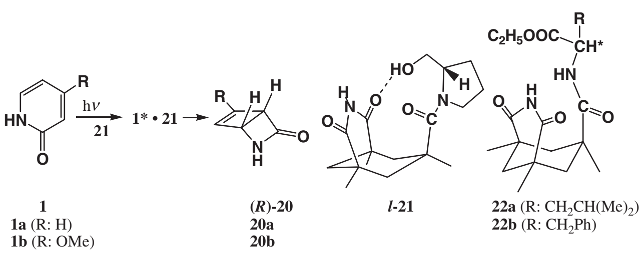

Figure 20. Photovalence-isomerization and host **22**.

however, requires half reduction of the imide carbonyls and optical resolution. Such a preparation is considered to be rather difficult. We show here the preparation of new imide-amide hosts **21** and **22** from easy coupling of Kemp's chloride with (*l*)-prolinol as presented in Scheme 16.[25]

Figure 19 presents the X-ray crystallographic data of the host (*l*)-**21** ($[\alpha]_D = -47.2°$ (MeCN)). As intended, the one imide carbonyl exhibits a moiety to make the imide group asymmetric. The next photochemistry and the other hosts **22a** and **22b** derived from natural amino acids are shown in Figure 20. The interaction between guest **1a** and chiral host **22b** was titrated by Job's plot of ^{1}H NMR in acetonitrile to be a 1:1 complex with a binding constant, $K_a = 91.3\,M^{-1}$. Photoirradiation of **1a** with **21** (or **22a**) in an acetonitrile solution gave photopyridone **20a** as follows.[25] The enantiomeric excess (%ee) was measured by a chiral HPLC column (CHIRALPAC AD/DAICEL). **1a** (1.0×10^{-2} M) and (*l*)-**21** (2.5×10^{-2} M) in $CHCl_3$ at room temperature gave **20a** (13%ee at 30% conversion). **1a** (1.0×10^{-2} M) and **22a** (5.0×10^{-2} M) in $CHCl_3$ at room temperature gave **20a** (42%ee at 30% conversion).

4.2 MO Analysis of the Intramolecular H-Bonding in Imide-Amide (*l*)-21, Intermolecular Host–Guest Phenomena between 1 and 21 and the Photoisomerization. Figure 21a is the optimized geometrical data of host **21** by PM3[46b] which is a better method for evaluating H-bonding. The

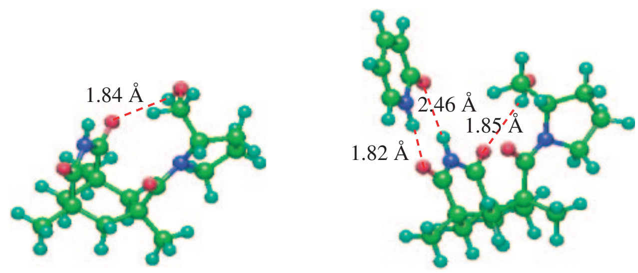

(a) (*l*)-**21** (b) **1a**· (*l*)-**21**

Figure 21. Optimized geometry of host (*l*)-**21** and molecular simulation of 1:1 complex by hydrogen-bondings between **1a** and host **21** by PM3.

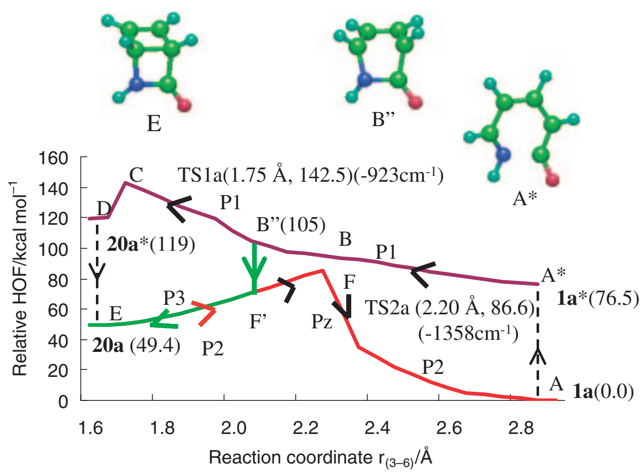

Figure 22. Molecular simulation of photoreaction process and energies on the photoisomerization from **1a** to **20a** (PM5).

structure shows an intramolecular chiral H-bond (C=O/HO = 1.84 Å) similar to the X-ray data in Figure 19.

The molecular simulation of the 1:1 complex between **1a** and **21** (CO/NH = 2.46 Å, NH/CO = 1.82 Å) was performed by approach of the two molecules to give the intended hydrogen-bonding and the conformation and energy are shown in Figure 21b.[25] From the energies of the host·guest **1a·21**, **1a** and **21**, the stabilization energy was estimated to be 4.0 kcal mol^{-1}. This energy was primarily due to the two H-bonds. Such interactions give rise to an enantiomeric valence-isomer (*R*)-**20** by one-sided disrotatory [4π]-electrocyclization as shown in Figures 22–24. The photovalence isomer **20** is derived from a short lived (ca. 0.2 ns) excited singlet state **1*** of **1** by irradiation above 300 nm.[32a,32f]

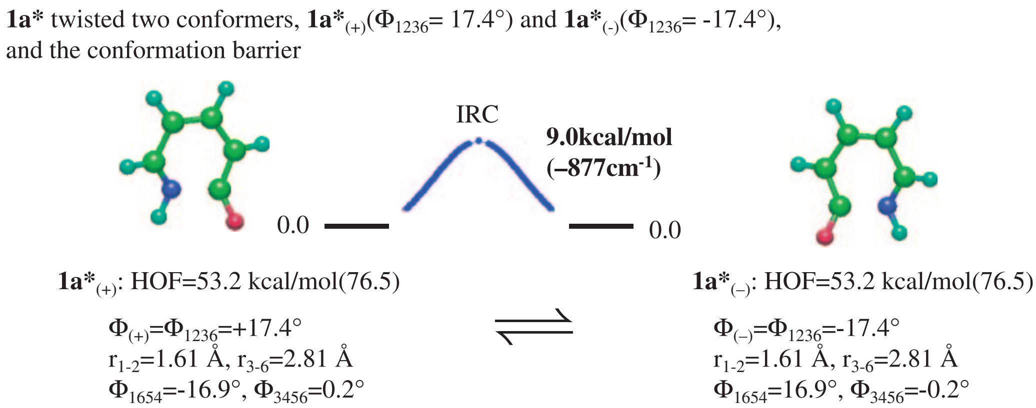

Figure 23. Conformation of excited singlet state **1a*** of 2-pyridone (**1a**) and the barrier.

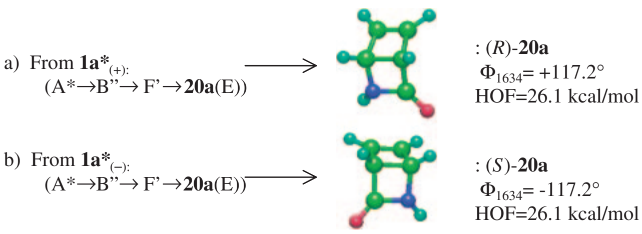

Figure 24. Selective valenceisomerization of pyridone excited singlet state **1a*** to the photopyridone **20a**.

Table 10. Potential Energies and Relative Energies of Pyridone **1** and Photopyridone **20**

Method	**1a** (**1b**)	**20a** (**20b**)
B3LYP$^{a)}$/au	−323.5331051	−323.3442677
rel. B3LYP/kcal mol^{-1}	0.0	56.7
PM5/kcal mol^{-1}	−23.3	26.1
rel. PM5/kcal mol^{-1}	0.0 (0.0)	49.4 (48.0)

a) Basis set: 6-31+G(d).

We first described the potential energy difference between **1a** and **20a**, properties of **1*** and the changing process from **1*** to **20**.[25b] Table 10 shows the potential energies of B3LYP/6-31+G(d) and PM5 levels. Examples of the energy deviation by the calculation methods are shown in some reports.[46] B3LYP and PM5 for TS analysis[21–24,46b–46d] and B3LYP and PM3 for H-bonding evaluation[46b,46d,47] may be reasonable. The energy difference in Table 10 is approximately twice the difference between norbornadiene and quadricyclane (NBD-QC), which are compounds being developed as solar energy storage and new switching systems.[48]

Figure 22 shows the molecular simulations of the photoreaction process and energies from **1** (**A**) (via **1*** (**A***)) to **20**(E), and the thermal process from **20** to **1**. They are composed of three processes (P1, P2, and P3). The horizontal axis shows the distance $r_{3\text{–}6}$(Å) of **1**, **1***, or **20**, and the vertical axis represents the relative potential energy HOF (rel. HOF; kcal mol^{-1}) at the reaction steps. The P1 process (violet line) goes from A* to D via gentle slope points, B and B″ (at 2.0 Å) and C. The C point shows the first transition state TS1 ($r_{3\text{–}6} = 1.75$ Å, rel. HOF = 142.7 kcal mol^{-1}, the negative number of vibration = −925 cm^{-1}). D quenches to E (**20**: 1.60 Å, 49.4 kcal mol^{-1}) by the deactivation keyword. Since the TS1 energy is 66 kcal mol^{-1} higher than **1***, the (**1*** → **20**) process just by P1 is actually impossible. The P2 process (red line) changes from **20** to **1** via the second transition state TS2 (F: 2.20 Å, 86.6 kcal mol^{-1}, −1385 cm^{-1}) at the ground state. Such pyrolysis data at 130–160 °C are available.[32b] We then searched the P3 process (green line) starting at B″ (2.0 Å, 105 kcal mol^{-1} on P1), followed by the deactivation keyword to F′ and the reaction went to E(**20**). Deactivation at B ($r_{3\text{–}6} = 2.2$ Å) showed a tendency to revert back to **1**. These phenomena show that three potential energy surfaces (PES) are concerned in the valence isomerization (**1** → **20**) and that the photoreaction process is as follows:

$$\mathrm{A}(\mathbf{1}) \xrightarrow{h\nu} \mathrm{A}^*(\mathbf{1}^*) \xrightarrow{\mathrm{P1}} \mathrm{B}'' \xrightarrow{\mathrm{P3}} \mathrm{F}' \xrightarrow{\textit{disrotatory}} \mathrm{E}(\mathbf{20}) \tag{5}$$

There is no overlap between B″ (on P1) and F′ (on P3 and P2) in Figure 22. The higher vibrational levels of P3 ($S_{0,n(n=1,2,3,\ldots)}$) may be overlapping with P1 ($S_{1,0}$),[49] and **1*** may quench to the isomer **20** (photopyridone). Photopyridone **20b** of 4-methoxy-2-pyridone (**1b**) was afforded at higher yield and the chiral lactam was utilized for β-lactams and carbocyclic oxetanocines which are used as HIV drugs.[32d,32e] The photoisomerization curve of **1b** by our simulation gave the more gentle P1 and a narrower gap for quenching to the photopyridone than presented in Figure 22.[25b]

We also estimated an enantiomeric conformation of the excited singlet pyridone **1***, indicating the presence of the two asymmetric conformers, **1***$_{(+)}$ and **1***$_{(-)}$. As shown in Figure 23, the (+)/(−) represents +17.4°/−17.4° of the dihedral angles, Φ_{1236} in the conformers. This shows two twisted energies, steric structures and the conformational barrier energy of 9.0 kcal mol^{-1}. Figure 24a shows a molecular simulation from **1***$_{(+)}$ to (*R*)-**20a**, in which selective disrotatory [4π]-electrocyclization occurred. (*R*)-**20a** corresponds to (1*R*,4*R*)-(+)-2-azabicyclo[2.2.0]hex-5-en-3-one after optical resolution by Hongo et al.,[32e] and by the chiral host–guest photolysis of Bach et al.[27a] In Figure 24b the molecular simulation verifies the formation of (*S*)-**20a** from **1***$_{(-)}$.

We next described the molecular simulations of the H-bonding properties of (*l*)-prolinol-amide imide host **21** ((*l*)-**21**), the complex **1**•(*l*)-**21** in Figure 21, the exciplex **1***•(*l*)-**21** and the chiral photovalence-isomerization to (*R*)-**20**.[25] Figure 25

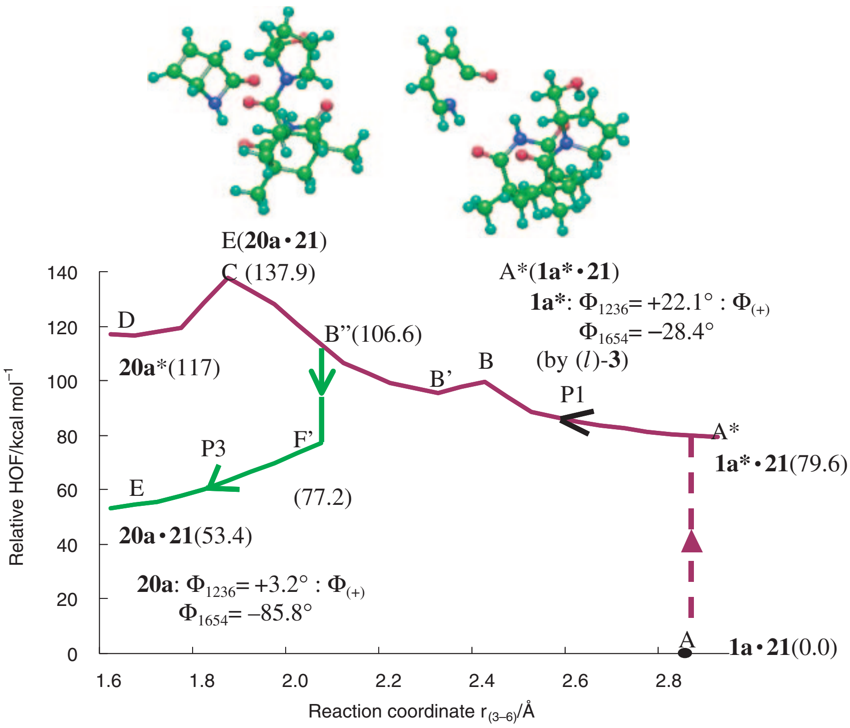

Figure 25. Molecular simulation of photoreaction process and energies on the valenceisomerization from **1a**$\cdot$(*l*)-21 to (*R*)-**20a** (PM3).

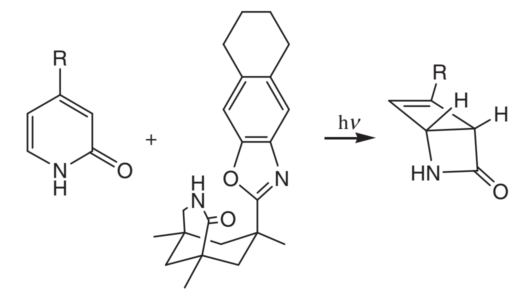

1
1a (R=H)
1b (R=OMe)

23

(*R*)-**20a**
(*R*)-**20b**

Scheme 17.

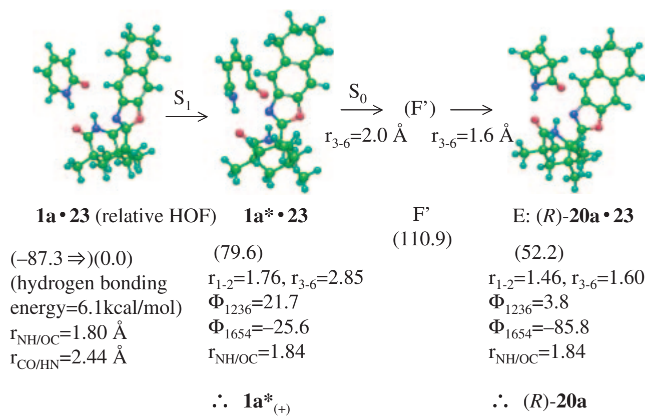

Figure 26. MO verification on the photoisomerization from **1a**$\cdot$**23** to (*R*)-**20a** (PM3).

shows the molecular simulation of the photovalence-isomerization from the complex **1***$\cdot$(*l*)-**21** to (*R*)-**20**$\cdot$(*l*)-**21**, followed by the release of (*R*)-**20**. Since the energy change is similar to that presented in Figure 22, the photoreaction process is represented as:

$$\mathbf{1} \rightarrow A(\mathbf{1}\cdot(l)\text{-}\mathbf{21}) \rightarrow \mathrm{A}^* \rightarrow \mathrm{B}'' \rightarrow \mathrm{F}' \rightarrow \mathrm{E}((R)\text{-}\mathbf{20}\cdot(l)\text{-}\mathbf{21}) \rightarrow (R)\text{-}\mathbf{20} \quad (6)$$

Namely, (*l*)-**21** was estimated to preferentially form a diastereomer $\mathbf{1}^*_{(+)}\cdot(l)$-**21** by the photoexcitation of **1**$\cdot$(*l*)-**21**, and to release (*R*)-**20** by the one-sided [4π]-electrocyclic rotation to a lower energy.

Such an estimation was confirmed by a similar simulation using the **1**$\cdot$(*d*)-**21** complex to release (*S*)-**20**.[25b]

We also simulated Bachs' experimental result in Scheme 17.[27a] In this study, the chiral host **23** was synthesized via reduction of Kemp's imide lactam and successive optical resolution, and the **1a**$\cdot$**23** complex to (*R*)-**20a** by photochemical isomerization was derived. Figure 26 shows the molecular simulation verification on the photoreaction from the **1a**$\cdot$**23** complex to (*R*)-**20a** via diastereomeric $\mathbf{1}^*_{(+)}\cdot\mathbf{23}$ and (*R*)-**20a**$\cdot$**23**.[25b] The reaction is recognized to be a one-sided disrotatory [4π]-electrocyclic reaction which involves smaller steric hindrance. Such dynamic molecular simulations of photoreactions suggest that our experimental **20a** in Section **4.1** is rich in (*R*)-**20a**, and that the analysis may be suitable for chirality determination of the reactants and products.

4.3 The Large Endothermic Photoreaction and Some Predictions. The energy storage of the endothermic photoreaction ($\mathbf{1} \rightarrow \mathbf{20}$) was estimated to be about 50 kcal mol^{-1}. This energy is twice that of the NBD-QC system. We then performed the following two types of molecular simulations.

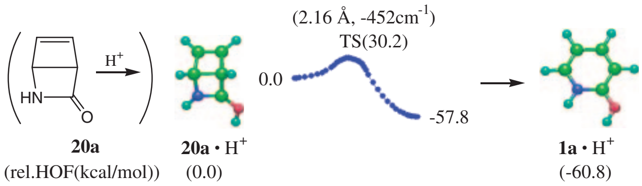

Figure 27. Molecular simulation of acid catalysis for back valenceisomerization (**20a** → **1a**) (PM5).

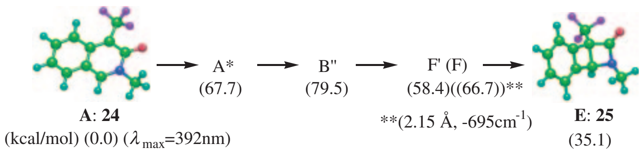

Figure 28. Molecular simulation data on photoreaction of *N*-methyl-1-trifluoromethyl-3-isoquinolone (**24**) to the valenceisomer **25**.

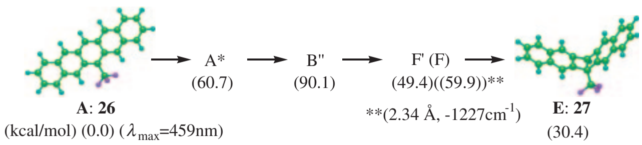

Figure 29. Molecular simulation data on photoreaction of 6-trifluoromethylpentacene (**26**) to the valenceisomer **27**.

4.3.1 Control of the Inverse Reaction (20 → 1): **20** is pyrolyzed at 160 °C to **1** and an unknown.[32b] For the recycle reaction (**1** → **20**), an acid catalytic action for the (**20** → **1**) reaction was simulated as shown in Figure 27.[25b] The TS energy decreased to 30.2 from 37.2 kcal mol^{-1} in Figure 22, and the energy gap between **20**•H$^+$ and **1**•H$^+$ advanced to 58 kcal mol^{-1}. Such acid treatment is recommended for the application of the reaction (**1** → **20**).

4.3.2 Valence Isomerization of 3-Isoquinolones and Pentacenes: The UV spectrum of 2-pyridone (**1**) showed a $\lambda_{max} = 300$ nm ($\log \varepsilon = 4$). Since solid 3,4,6-triphenyl-2-pyridones showed blue fluorescence stronger than pyrene,[50] the phenomena is very interesting. The λ_{max} (=340 nm) is however thought to be inadequate for solar light absorption. Figure 28 shows the molecular simulation data of the photovalence-isomerization from *N*-methyl-1-trifluoromethyl-3-isoquinolone (**24**)[51] to the valence isomer **25**. The symbols have the same definition used in Figure 22. The λ_{max} (calcd) = 392 nm ($\pi \to \pi^*$) suggests absorption of visible light. The smaller energy gaps (12.6 and 31.6 kcal mol^{-1}) of A* and B$''$, and E and F than that presented in Figure 22 suggest that **24** may be active for solar-energy storage and suitable as recycler materials. Figure 29 shows similar molecular simulation data of 6-trifluoromethylpentacene (**26**) for the valence isomer **27**. The pentacene absorbs wide visible light and has been developed as organic electroluminescence material. **26** holds promise for use in solar-light sensitive materials.

4.4 Conclusion on the Photovalence-Isomerization. Endothermic formation of chiral photopyridone **20** from **1** is very interesting in photoreaction theory, chiral synthesis and solar-energy storage. Prepared chiral imide-amide host (*l*)-**21** forms a H-bonding complex **1**•(*l*)-**21**, which is followed by photoreaction to give (*R*)-**20**. Molecular simulation of the excited singlet state **1*** showed **1*** exists as two conformers (**1***$_{\Phi(+)}$ and **1***$_{\Phi(-)}$: $\Delta E_K = 8$–9 kcal mol^{-1}) which are non-planer and enantiomeric, and 1*$_{\Phi(+)}$ was shown to go to (*R*)-**20** via three kinds of potential energy surfaces (PES).

Formation of (*R*)-**20a** by photoreaction of the **1a**•(*l*)-**21** complex was simulated to be introduced to **1***$_{\Phi(+)}$•(*l*)-**21** by S_1 excitation of the **1a**•(*l*)-**21** followed by a decrease of the $r_{3\text{-}6}$ and deactivation to (*R*)-**2a**. We verified that the **1a**•(*d*)-**21** singlet excitation gives (*S*)-**20a**, and that the molecular simulation of **1**•**23** host–guest experiments by Bachs' also gives (*R*)-**20**.

Moreover, we checked the large energy-storage, substituent effect and acid-catalyst effect for the **1** → **20** recycle reactions and propose new solar energy-storage and switching systems.

5. Molecular Simulation of Enantiodifferentiating Photoisomerization of Cyclooctene (28Z) by Chiral Sensitizers 30

5.1 Chiral Control and Enantiodifferentiating Photoisomerization of 28Z to Chiral (*E*)-Cyclooctene (29E) by Sensitizers. The origin of biomolecular homochirality under sunlight is one of the most contentious subjects in chemistry. The field of asymmetric photochemistry has undergone accelerated development only in the past 20 years. *Chiral Photochemistry*, ed. by Y. Inoue, V. Ramamurthy provides a range of articles with various aspects of controlling the chirality of photochemical reactions.[30a] The monograph contains: (1) direct asymmetric photochemistry with circularly polarized light, (2) enantiodifferentiating photosensitized reactions, and (3) enantioselective photochemical reactions in various molecular aggregates. However, very few authors describe the chiral mechanisms using an MO method.

Various and interesting experimental studies by Inoue et al. on the enantiodifferentiating photosensitized reactions in solution,[28–30] have stimulated our interest in understanding the mechanism and factors that control the enantio- and diastereo-differentiating processes. In particular, the sensitized enantioselective photoisomerization actions by chiral benzenecarboxylates **30** presented in Scheme 18 were especially appealing as a method for efficient chirality transfer in solution. We have elucidated major factors and the origin for many types of stereoselective photoadditions[22–24] and photovalence-isomerizations.[25] We now estimate the energy and stereochemical profile of the sensitized (Z–E)-isomerization of cyclooctene **28Z** by the excited singlet states of some benzenepolycarboxylates **30b**–**30d** in Scheme 18[28–30] using molecular simulation at primarily the PM5 level.[26] The photosensitized isomerization process is presented as the solid line via 2 exciplexes, **Ex1** and **Ex2** in Figure 30.

The sensitized photoisomerization data of **28Z** to **29E** by many kinds of benzenecarboxylates are given in the literature as the following.[28–30]

(1) The **29E**/**28Z** ratio by **30a**, **30b**, **30c**, and **30d** are nearly 0.01, 0.1, 0.6, and 0.3, respectively.

(2) The enantioselectivity, (*S*)-**29E**/(*R*)-**29E** ratio by **30a** is higher than the value derived by **30d**.

5.2 Molecular Simulation of Enantioselective Photoisomerization of 28Z by 30.[26] **5.2.1 Calculations, Energy**

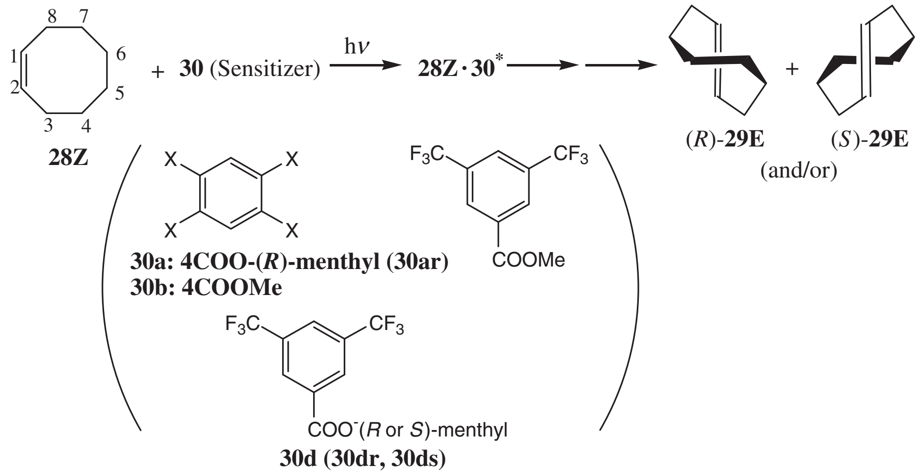

Scheme 18.

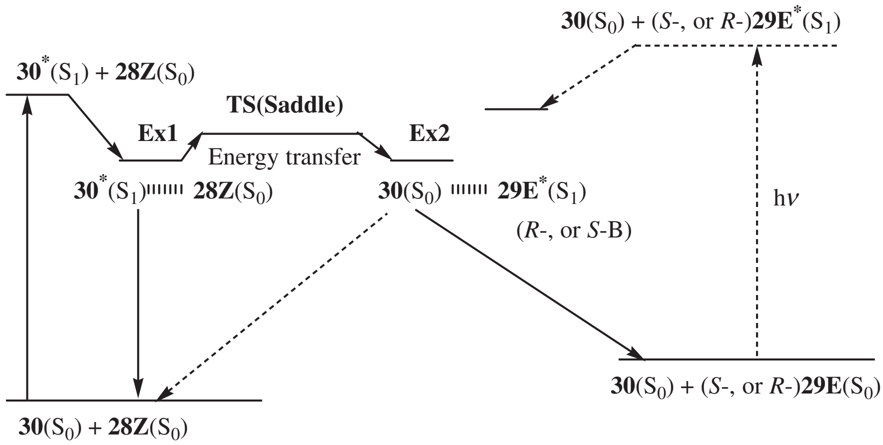

Figure 30. Process of sensitized enantiodifferentiating photoisomerization.

(HOF) Diagram, and Stereochemical Profile of 28Z, 29E, and the Sensitizers 30: After geometry optimization of **28Z**, **29E**, and **30**, and their excited singlet states (**28Z***, **29E***, and **30***), interactions between **28Z** and **30*** were calculated by approach of the proper parts of the two molecules, to generate the existence of exciplexes (**Ex1**) and to pass the transition state (TS1). The HOF of the lowest energy conformer of **28Z** by the PM5 method is $-14.7\,\mathrm{kcal\,mol^{-1}}$. This energy value is $11.7\,\mathrm{kcal\,mol^{-1}}$ lower than that of **29E** (dihedral angle: $\Phi_{8123} = 143°$). Their relative results and stereochemistry are presented in Figure 31.

28Z ($\Phi_{8123} = -1.5°$, $\Phi_{4567} = -107°$) was analyzed to have the asymmetric conformer **28Zc** ($\Phi_{8123} = 1.5°$, $\Phi_{4567} = 107°$), and a conformation barrier ($4.9\,\mathrm{kcal\,mol^{-1}}$) for equilibrium (Scheme 19) may be concerned with the chiral sensitization by chiral sensitizers as shown in Section **5.2.3**.

The TS point (relative HOF $= 61\,\mathrm{kcal\,mol^{-1}}$) between **28Z** and **29E** in Figure 31 was introduced by use of the keyword SADDLE, and then TS. The two excited singlet states (**28Z*** and **29E***) are intersected at $\Phi_{8123} = 94°$, and have other conformers. Figure 31 also explains the population data (**28Z**/**29E** $= 0.5$) at the direct photoisomerization presented by Inoue et al.[30]

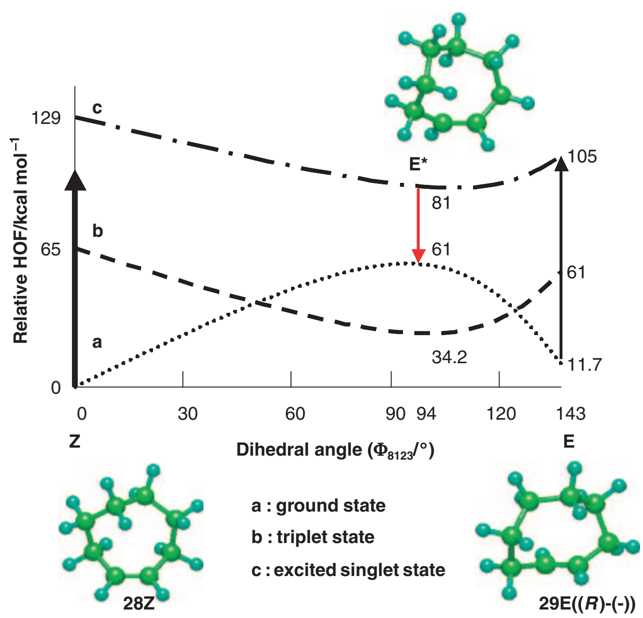

Figure 31. Relative energy (HOF) versus dihedral angle of **28Z** and **29E**.

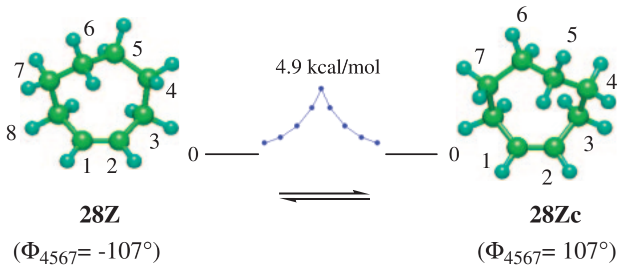

Scheme 19.

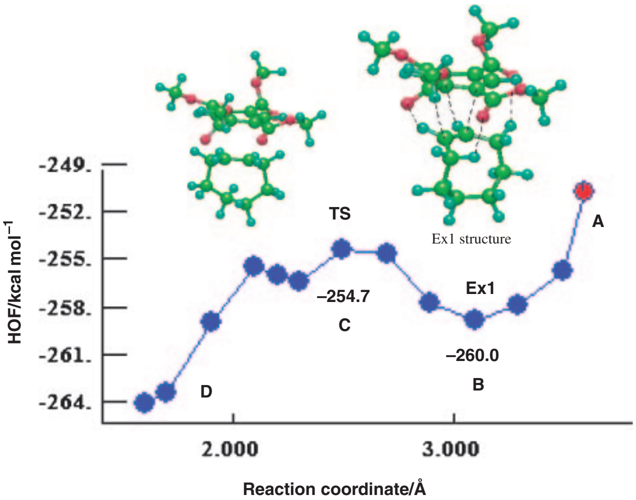

Figure 32. Interaction between **28Z** and **30b***.

5.2.2 Sensitized Photoisomerization of 28Z to 29E by 30b* (and by 30c*): Figure 32 shows the existence of exciplex **Ex1** (**28Z·30b***: B) formation by approach between C1(**30b***) and C1(**28Z**). Such phenomena are explained by the following eq 7:

$$(\mathbf{28Z} + \mathbf{30b} \xrightarrow{h\nu}) \ \mathbf{28Z} + \mathbf{30b}^* \rightarrow \mathbf{28Z{\cdot}30b}^* \ (\mathbf{Ex1}) \qquad (7)$$

The HOF of **Ex1** is 34 kcal mol^{-1} lower than the sum of (**28Z** + **30b***), and nothing of the photoadduct via a biradical (D), which is also similar to the biradical D in Figure 33, is explained by the high barrier (C).

The stabilization of **Ex1** is inferred from the π–π* interaction, four H-bonds and C–H/π[47a] interactions between the carbonyl oxygens or π components and C(π)–H or allylic hydrogens observed in B conformation **Ex1**. The dihedral angle Φ_{8123}(**28Z**) in B was twisted (20°). We subsequently checked two possibilities of: (a) ground state isomerization of eq 8:

$$\mathbf{28Z{\cdot}30b}^* \rightarrow \mathbf{29E{\cdot}30b}^* \qquad (8)$$

and (b) energy transfer of eq 9:

$$\mathbf{28Z{\cdot}30b}^* \rightarrow \mathbf{29E}^*\mathbf{{\cdot}30b} \qquad (9)$$

For (a) the change to 94° of the dihedral angle Φ_{8123}(**28Z**) in **28Z·30b*** similar to Figure 32 required a significant energy, 49 kcal mol^{-1}, which indicates that this process is impossible. We next calculated the energy for (b).

Figure 34 shows the interaction between **29E*** and **30b** for **Ex2** formation in eq 9. The **Ex2** energy (−257 kcal mol^{-1}) is 15 kcal mol^{-1} lower than the total energy of **29E*** and **30b**, and 3 kcal mol^{-1} higher than the energy of **Ex1** in Figure 32. **Ex2** is followed by quenching to **29E** (and **28Z**). These data may be used for the explanation of the **E**/**Z** ratio = 0.1 at the (**28Z** + **30b**) photoreaction.

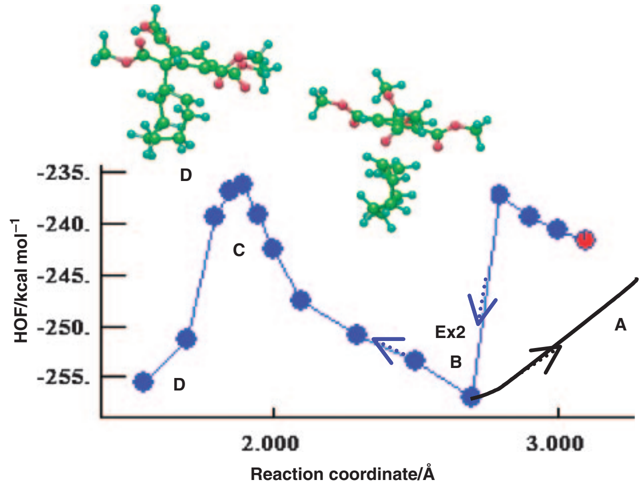

Figure 33. Interaction between **29E*** and **30b**.

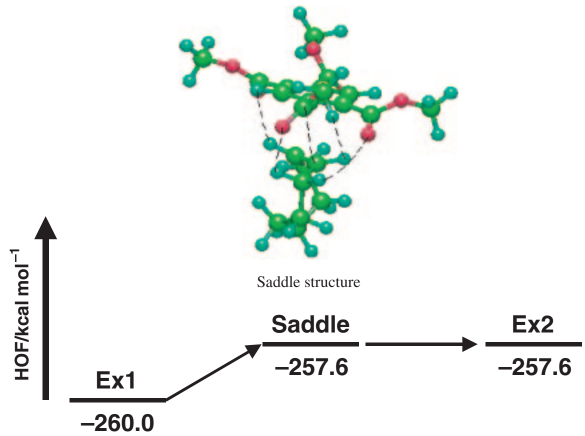

Figure 34. Energy transfer from **28Z·30b*** (**Ex1**) to **29E*·30b** (**Ex2**).

We also simulated the transition process from **Ex1** (**28Z·30b***) to **Ex2** (**29E*·30b**) by using the PM5 keyword, SADDLE, and present the data in Figure 34. The saddle structure in Figure 34 has the following data:

29E: $\Phi_{8123} = -121.8°$, $\Phi_{4567} = -59.2°$, r(1(**29E**)–1(**30b**)) = 2.82 Å, r(2(**29E**)–2(**30b**)) = 3.30 Å, r(2(**29E**)–5(**30b**)) = 2.94 Å, r(CH–O=C) = 2.50, 2.69, 2.75, 2.89 (Å), r(1-H(**29E**)–1(**30b**)) = 2.39 Å, r(2-H(**29E**)–4(**30b**)) = 2.46 Å.

The data are near to those of **Ex1** except Φ_{8123}, and similar to a singlet exciplex of the [3 + 2] addition type. Since the TS energy is very low, the energy transfer equilibrium is smooth and thought to be caused by multiple H-bonds and CH–π interactions (the distances: 2.3–2.9 Å) at the TS state.

The sensitized photoisomerization of **28Z** to **29E** by use of **30c** was examined[30] and the molecular simulation is explained by energies and stereochemical changes of the energy transfer from **28Z·30c*** (**Ex1**) to **30E*·30c** (**Ex2**). The **29E**/**28Z** ratio of the sensitized reaction of **28Z** to **29E** by **30c** is relatively high (**E**/**Z** = 0.6). The calculated energy diagram and stereo-

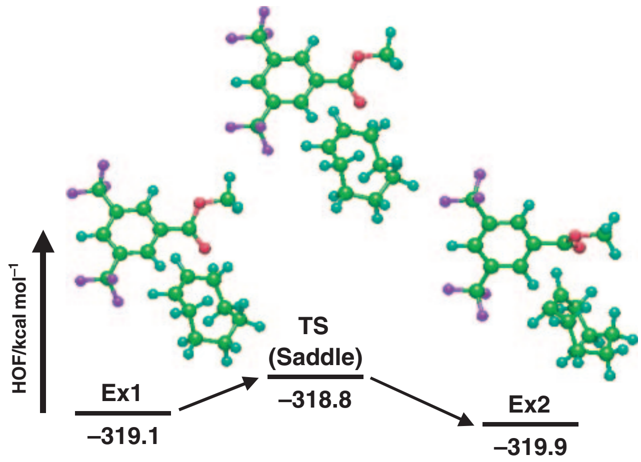

Figure 35. Energy transfer from **28Z·30c*** (**Ex1**) to **29E*·30c** (**Ex2**).

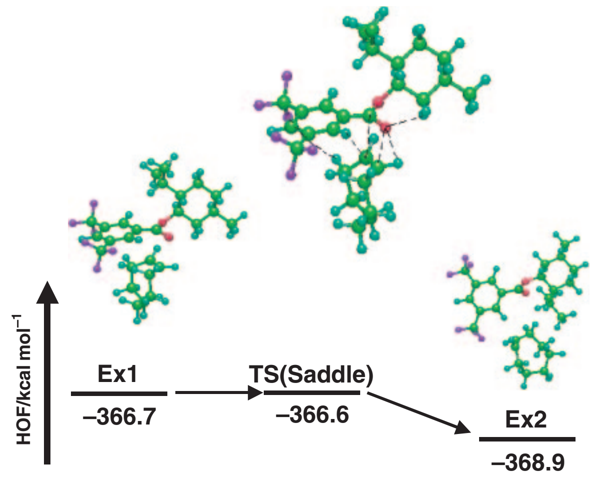

Figure 36. **Ex1** and **Ex2** from reaction (**28Z** + **30dr**) and the energy transfer.

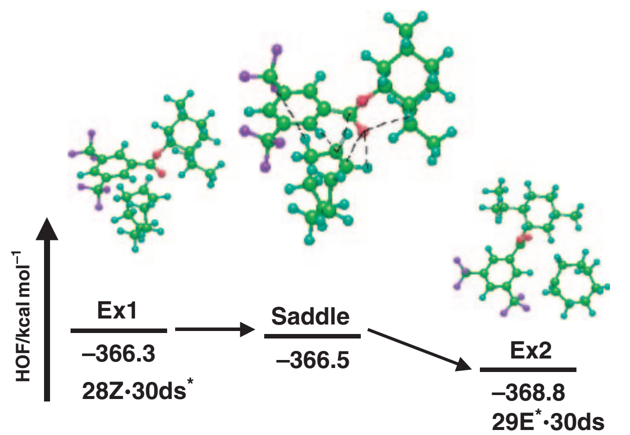

Figure 37. **Ex1** and **Ex2** from reaction (**28Z** + **30ds**) and the energy transfer.

chemistry by approach between C2 (**30c***) and C1 (**28Z**) suggest the formation of the exciplex **28Z·30c*** (**Ex1**) and HOF (-319.1 kcal mol^{-1}), which is 32 kcal mol^{-1} lower than the initial material (**28Z** + **30c***). The stabilization is taken from the H/F H-bonding present alongside. In the interaction (**29E*·30c**: -319.1 kcal mol^{-1}) between **29E*** and **30c** for **Ex2**, **29E*** is alongside **30c** due to H-bonding, CH/π and H/F. The energy transfer data in Figure 35 (TS: -318.8 kcal mol^{-1}) from **Ex1** (**28Z·30c***) to **Ex2** (**29E*·30c**) by use of the keyword, Saddle, suggest that the isomerization is very smooth. The **29E**/**28Z** ratio by **30c** is larger than that by **30b**. From the experimental data and Figures 34 and 35, **Ex1** > **Ex2** in energy (HOF) and this leads to the high **29E**/**28Z** ratio.

5.2.3 Chiral Isomerization of 28Z to 29E by Chiral Menthyl 3,5-Bis(trifluoromethyl)benzoate (30d): 5.2.3.1 Isomerization by (*R*)-Menthyl Isomer 30dr; An approach between the excited singlet state **30dr*** and **28Z** using the PM5 program showed the existence of the exciplex **28Z·30dr*** (**Ex1** in Figure 36) (HOF = -366.7 kcal mol^{-1}, dihedral angle Φ_{8123}(**28Z**) = $-21.4°$) which is 16.9 kcal mol^{-1} lower than the total energy of (**28Z** + **30dr***). A similar approach between the excited singlet state **29E*** and **30dr** showed the existence of the exciplex **29E*·30dr** (**Ex2** in Figure 36) (HOF = -368.9 kcal mol^{-1}), which is 4.5 kcal mol^{-1} lower than the total energy of (**29E*** + **30dr**), and 2.1 kcal mol^{-1} lower than **Ex1**. The transition simulation from **Ex1** (**28Z·30dr***) to **Ex2** (**29E*·30dr**) by the keyword (Saddle) showed the TS energy (-366.6 kcal mol^{-1}) and the steric conformation in Figure 36. Since the TS energy is very small (0.1 kcal mol^{-1}), the energy transfer leading to the isomer **29E** is inferred to be similar to the case of **30c**. The dihedral angle Φ_{8123}(**28Z**) also changed from -21.4 to $-34.2°$ and $-85.2°$ during the transfer, which suggests a change to (*R*)-**29E** ($\Phi_{8123} = -143°$) by a one-sided rotation.

The other exo-approach between cyclooctene and the benzene ring of **30dr*** showed a smaller stabilization (2.2 kcal mol^{-1}) than the previous approach (16.9 kcal mol^{-1}).

5.2.3.2 Isomerization by (*S*)-Menthyl Isomer 30ds and Enantiodifferentiation; A similar approach between the unstable excited singlet state **30ds*** and **28Z** showed the existence of the exciplex **28Z·30ds*** (**Ex1** in Figure 37) (HOF = -366.3 kcal mol^{-1}, $\Phi_{8123} = -29.3°$), which is 0.4 kcal mol^{-1} unstable when compared with **28Z·30dr*** in (1). The exciplex **29E*·30ds** (**Ex2** in Figure 37) (HOF = -368.8 kcal mol^{-1}) between **29E*** and **30ds** is 2.5 kcal mol^{-1} lower than **Ex1**.

The transition simulation from **Ex1** to **Ex2** in Figure 37 showed a low TS energy (-366.5 kcal mol^{-1}). The energy value is almost the same as **Ex1**. By comparison of Figures 36 and 37, **28Z** ($\Phi_{8123} = -1.5°$) appears to be introduced more effectively to **Ex1** and **Ex2** by **30dr** than **30ds**, and to be followed by (*R*)-**29E** ($\Phi_{8123} = -143°$), which was examined experimentally by Inoue et al.[29,30] The enantiodifferentiation may come from the proper intermolecular H-bond interactions between π-H or allyl groups in **29Z**, and asymmetric ester carbonyl in **30dr**. The CF_3 groups in **30dr** are also thought to be effective for the interactions in the stereochemistry.

5.2.3.3 Comparative Advantage between Figures 36 and 37; The structural data of the former and the latter are as follows. **Saddle**/(**28Z** + **30dr**): $\Phi_{8123} = -33.4°$, $\Phi_{4567} = -109.8°$, r(1(**28Z**)–1(**30dr**)) = 3.32 Å, r(1(**28Z**)–2(C=O)) = 3.02 Å, r(2(**28Z**)–2(O=C)) = 2.63 Å, r(CH–O=C) = 2.34, 2.46 (Å), r(CH/F) = 3.06 Å, **28Z**/isopropyl **30dr**: *exo*.

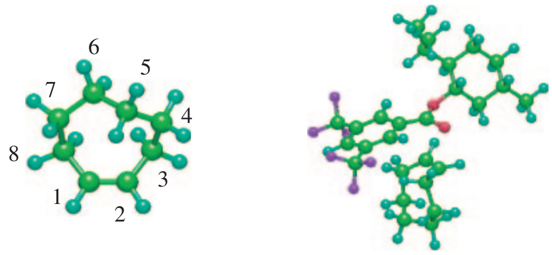

Figure 38. **28Zc** and the **Ex1** (**28Zc·30ds***) from reaction (**28Zc** + **30ds**).

Saddle/(28Z + 30ds): $\Phi_{8123} = -28.2°$, $\Phi_{4567} = -109.8°$, r(1(**28Z**)–1(**30ds**)) = 3.32 Å, r(1(**28Z**)–2(C=O)) = 3.07 Å, r(2(**28Z**)–2(O=C)) = 2.71 Å, r(CH–O=C) = 2.45, 2.57 (Å), r(CH/F) = 2.99 Å, **28Z**/isopropyl **30ds**: *endo*.

The saddle/(**28Z** + **30dr**) appears to have advantages in π–π^* and H-bonding interactions, ionic interactions by ester carbonyl and steric and conformational factors by the isopropyl group. The smaller r(CH/F) in the latter **saddle** also suggests a delicate balance between their interactions and steric factors. The interaction balance provides a smaller advantage in Φ_{8123} of the former, which is followed by (R)-**29E**.

5.2.3.4 Simulation by Use of Conformational Isomer 28Zc (Φ_{4567} = 107°); As shown in Figure 38, the isomer **28Zc** was simulated to become rich (S)-**29E** or not by use of **30ds**. Thus the energy **Ex1** (**28Zc·30ds***) (−366.5 kcal mol^{-1}) was lower than of the energy of the diastereomeric exciplex **Ex1** (**28Zc·30dr***) (−364.4 kcal mol^{-1}). The latter data also suggests some margin of error.[22b,46] By comparison of three steric structures of **Ex1** in Figures 36, 37, and 38, we infer that the isopropyl group in the menthyl substituent is more of a hindrance than an interaction.

Pirrung et al.[52] recently demonstrated that (R)-riched (E)-cyclooctene (**29E**), which was prepared by Inoue et al., was more effective than the (S)-riched **29E** as the ethylene receptor (ETR1) antagonist. Since ethylene is used as a hormone to control particular physiological processes in plants, the enantiomeric selectivity may provide a search approach for the asymmetric ETR1 protein-composed environment.

5.3 Conclusion on the Enantiodifferentiation. Interesting experimental results for enantiodifferentiating photoisomerization of (Z)-cyclooctene (**28Z**) to chiral E isomer **29E** sensitized by chiral polyalkyl benzenepolycarboxylates **30a–30d** were elucidated on the energy and stereochemical profiles derived from a molecular simulation using the MOPAC-PM5 program.

Energy, stereochemistry and the equilibria of the ground states of **28Z** (and conformer **28Zc**), **29E**, **30b–30d** and the excited singlet states of **28Z***, **29E***, **30*** were first elucidated. One asymmetric conformer **28Z** ($\Phi_{4567} = -107°$) was inferred to have the preferential one-sided rotation to form (R)-**29E** ($\Phi_{8123} = -143°$) by photoisomerization. The photoisomerizations between **28Z** and **30** were inferred to proceed via two exciplexes **Ex1** (**28Z·30***) and **Ex2** (**29E*·30**). The transition state (TS) for the energy transfer process is low and it is followed by quenching to **29E**.

The sensitization ratio **E/Z** may be related to the energy difference (ΔHOF) between each **Ex1** and **Ex2** as follows. Since **30b** gives a stable **Ex1** due to the π^*–π and four ester-carbonyls for the effective formation of intermolecular interactions including C=O/HC (π and allyl) H-bonding, the **E/Z** ratio is low (0.1). Since **30c** gives a stable **Ex2** because of the alongside interactions by the *meta*-CF_3 and ester carbonyl for **Ex2**, the **1E/1Z** ratio is relatively high (0.6).

The enantiodifferentiating photoisomerization of asymmetric **28Z** to chiral **29E** by chiral **30** may be estimated by calculating the diastereomeric **Ex1** energy and the TS energy for **Ex2**. The enantiomeric (R)-**29E** via low **Ex1** and a small TS process from **28Z** by **30dr** (or **28Zc** by **30ds**) was speculated to be the preferred route. The preference depends on the sum of the steric interaction and repulsion energies including H-bonding between the asymmetric **28Z** and the enantiomeric **30d***. The preference will be influenced by the **30d** substituents and the environment. Those accumulating interactions are inferred to bring enantiodifferentiating energy transfer by a one-sided rotation (asymmetric environment) of the two molecules for (R)-**29E** or (S)-**29E** like enzymes.

Such various and weak interactions are caused from intra- and intermolecular interactions and entropy-control factors such as the reaction temperature, and may influence the chirality control of the photosensitized isomerization in solution.

6. Concluding Remarks

We have studied the origins of photocycloaddition selectivities and of chirality controls in interesting and challenging photoreactions. Such mechanisms had not been characterized by only FMO methods, because they are essential for reaction theory and synthetic use. In this account, we described the profiles of energies and stereochemical changes in the following four types of photoreactions by molecular simulation using primarily MOPAC-PM5 (PM3 for H-bonding), UCIS (for excited singlet), and UB3LYP (for triplet) levels. Such a molecular simulation approach gave coarse but valuable conclusions (numbers in parentheses are relative energies).

(1) Photocycloadditions of five selectivity types (Sections **2.1–2.5**). (i) Anti-ht-[4 + 4]cycloaddition of singlet **1** (**1s**): The lower energy excimer and TS1 by the ionic interaction effects were discussed (Scheme 2). (ii) Endo-3,4-ht-[2 + 2]cycloaddition of singlet **1** (**1s**): The lower TS1 is presented by the concerted TS interaction by π–π^* interactions (Scheme 4). (iii) Exo-5,6-hh-[2 + 2]cycloaddition of triplet **1** (**1t**): The twisted TS1 structure forms by repulsive conformation but small energies are characteristic (Scheme 6). (iv) Inversion of regioselectivity (hh/ht ratio) in intramolecular [2 + 2]cycloadditions of triplet **7a** and **7b** (**7t**): The repulsive but smaller TS1 conformation energy for each regio-adduct is characteristic (Scheme 8). (v) Inversion of regioselectivity in intermolecular [2 + 2]cycloadditions of triplet **10** (**10t**) is dependent on the cycloalkene ring-size: The alkene deformation energy (ΔE_{df}-alkene) on the TS1 conformation is largely dependent on the increment of the ring-size, the hh conformation and was subject to ht adducts (Scheme 11).

(2) The occurrence of the hydrogen-shift in the case of triplet **17** (**17t**) and **18o**: The reaction pathway can be controlled by the intermolecular H-bonding at the TS1 state (Scheme 12).

(3) Chiral [4π]-electrocyclization of **1** to **20** by chiral amide host **21**: The existence of the two enantiomeric conformers of excited singlet state **1*** was elucidated and intermolecular H-bonding in the diastereomeric complex **1*·21** was observed in one-sided disrotatory electrocyclization to give chiral photopyridone **20** (Figures 22 and 25).

(4) (Z–E)-Isomerization of **28Z** and the chiral control for **29E**: Existence of double minima conformers and following diastereomeric exciplex by π–π^*, CH–π and C=O–H interactions with chiral sensitizer **28Z·30*** occurred in the one-sided isomerization to chiral **29E** (Scheme 19 and Figure 36).

The molecular simulations for the photoreactions are coarse, yet essentially successful. The simulations showed that the origin and/or chirality information of the selectivities is essentially determined by the TS1 energies and stereochemistries. The excited singlet reactions are in Figures 2–5, 22–26, 28, and 29 and involve attractions by particular interactions between the reaction parts. The triplet ones in Figures 6–12, 14, 15, 17, and 18 involve repulsions by the conformations. Some H-bonding in the reactions changes the product distributions. The finding that the energy and stereochemistry information is dependent on the excited species and on the TS1 is revealing. Such findings may provide a prospective sense of the photochemical reactions and some predictions for the chirality and possible applications.

The authors are grateful to their co-workers, who represent advisers and students within the groups, for the contribution to the photoreactions and the MO calculations found within their papers. The authors also thank Ms. Tomoko Ooto at the Faculty of Engineering of Kagoshima University for her valuable information and paperwork on the MO research.

References

1 *CRC Handbook of Organic Photochemistry and Photobiology*, 2nd ed., ed. by W. Horspool, F. Lenci, CRC Press, London, **2004**.

2 *Chiral Photochemistry*, ed. by Y. Inoue, V. Ramamurthy, Marcel Dekker, New York, **2004**.

3 a) J. D. Winkler, M. B. Rouse, M. F. Greaney, S. J. Harrison, Y. T. Jeon, *J. Am. Chem. Soc.* **2002**, *124*, 9726. b) N. Hoffmann, *Chem. Rev.* **2008**, *108*, 1052. c) D. Albrecht, B. Basler, T. Bach, *J. Org. Chem.* **2008**, *73*, 2345. d) Y. Yokoyama, *Kokagaku* **2008**, *39*, 162.

4 S. Tomoda, *Frontier Orbital Control, The World of Molecules*, Kodansha KK., Tokyo, **2007**.

5 R. B. Woodward, R. Hoffmann, *The Conservation of Orbital Symmetry*, Academic Press, Weinheim, **1970**.

6 I. Fleming, *Frontier Orbirals and Organic Chemistry Reactions*, John Wiley & Sons, Ltd., London, **1976**.

7 N. S. Allen, N. W. A. Geraghty, A. Gilbert, W. M. Horspool, in *Photochemistry*, ed. by I. Dunkin, The Royal Society of Chemistry, **2007**, Vol. 36, and the other volumes.

8 I. Fleming, *Frontier Orbital and Organic Chemistry Reactions*, translated by K. Fukui, Y. Takeuchi, S. Tomoda, Kodansha KK., Tokyo, **1978**, pp. 249–250.

9 a) D. I. Schuster, *Chem. Rev.* **1993**, *93*, 3. b) D. I. Schuster, in *CRC Handbook of Organic Photochemistry and Photobiology*, 2nd ed., ed. by W. Horspool, F. Lenci, CRC Press, London, **2004**, Chap. 72-7.

10 T. Bach, M. Kemmler, E. Herdtweck, *J. Org. Chem.* **2003**, *68*, 1994.

11 a) G. L. Lange, M. G. Organ, M. Lee, *Tetrahedron Lett.* **1990**, *31*, 4689. b) M. Tada, Y. Nieda, *Bull. Chem. Soc. Jpn.* **1988**, *61*, 1416.

12 K. Somekawa, T. Shimo, K. Tanaka, S. Kumamoto, *Chem. Lett.* **1975**, 45.

13 T. Suishu, T. Obata, T. Shimo, K. Somekawa, *Nippon Kagaku Kaishi* **2000**, 167.

14 K. Somekawa, H. Okuhira, M. Sendayama, T. Suish, T. Shimo, *J. Org. Chem.* **1992**, *57*, 5708.

15 T. Shimo, K. Somekawa, *Photocycloaddition Reactions of 2-Pyrones*, in *CRC Handbook of Organic Photochemistry and Photobiology*, 2nd ed., ed. by W. Horspool, F. Lenci, CRC Press, London, **2004**, Chap. 82-1.

16 T. Shimo, K. Sato, W. Wang, T. Obata, T. Iwanaga, T. Shinmyozu, K. Somekawa, *Bull. Chem. Soc. Jpn.* **2008**, *81*, 894.

17 K. Somekawa, R. Hara, K. Kinnami, F. Muraoka, T. Suishu, T. Shimo, *Chem. Lett.* **1995**, 407.

18 K. Somekawa, H. Oda, T. Shimo, *Chem. Lett.* **1991**, 2077.

19 W. Wang, T. Shimo, T. Shinmyozu, T. Iwanaga, K. Somekawa, *Hetrocycles* **2006**, *68*, 1381.

20 H. Miyauchi, C. Ikematsu, T. Shimazaki, S. Kato, T. Shinmyozu, T. Shimoi, K. Somekawa, *Tetrahedron* **2008**, *64*, 4108.

21 S. Kiri, Y. Odo, H. I. Omar, T. Shimo, K. Somekawa, *Bull. Chem. Soc. Jpn.* **2004**, *77*, 1499.

22 a) H. I. Omar, Y. Odo, Y. Shigemitsu, T. Shimo, K. Somekawa, *Tetrahedron* **2003**, *59*, 8099. b) Y. Odo, T. Shimo, K. Hori, K. Somekawa, *Bull. Chem. Soc. Jpn.* **2004**, *77*, 1209.

23 H. I. Omar, T. Shimo, K. Somekawa, *THEOCHEM* **2006**, *763*, 115.

24 D. Tokunaga, T. Shimo, H. Hashimoto, T. Ooto, K. Somekawa, *J. Comput. Chem. Jpn.* **2007**, *6*, 283.

25 a) K. Somekawa, T. Shimo, Y. Odo, D. Tokunaga, International Symposium. Advances in Supramolecular Chemistry, Strasbourg **2005**, Abstr. p. 42. b) K. Somekawa, Y. Odo, T. Ooto, H. Hashimoto, J. Miyauchi, T. Shimo, *J. Comput. Chem. Jpn.*, submitted.

26 H. Hashimoto, T. Shimo, M. Atsuchi, M. Mitsushio, K. Somekawa, *J. Comput. Chem. Jpn.* **2008**, *7*, 135.

27 a) T. Bach, H. Bergmann, K. Harms, *Org. Lett.* **2001**, *3*, 601. b) T. Bach, H. Bergmann, B. Grosch, K. Harms, *J. Am. Chem. Soc.* **2002**, *124*, 7982. c) B. Grosch, C. N. Orlebar, E. Herdtweck, W. Massa, T. Bach, *Angew. Chem., Int. Ed.* **2003**, *42*, 3693. d) T. Bach, B. Grosch, T. Strassner, E. Herdweck, *J. Org. Chem.* **2003**, *68*, 1107.

28 Y. Inoue, *Enantiodifferentiating Photosensitized Reactions*, in *Chiral Photochemistry*, ed. by Y. Inoue, V. Ramamurthy, Marcel Dekker, New York, **2004**.

29 a) Y. Inoue, T. Yokoyama, N. Yamasaki, A. Tai, *Nature* **1989**, *341*, 225. b) Y. Inoue, N. Yamasaki, T. Yokoyama, A. Tai, *J. Org. Chem.* **1992**, *57*, 1332.

30 a) *Chiral Photochemistry*, ed. by Y. Inoue, V. Ramamurthy, Marcel Dekker, New York, **2004**, pp. 129–178. b) T. Mori, Y. Inoue, *CRC Handbook of Organic Photochemistry and Photobiology*, 2nd ed., ed. by W. Horspool, E. Lenci, CRC Press, **2003**, Chap. 16-1.

31 Y. Odo, T. Shimo, M. Kawaminami, K. Somekawa, *Anal. Sci.: X-ray Struct. Anal. Online* **2004**, *20*, x119.

32 a) L. J. Sharp, IV, G. S. Hammond, *Mol. Photochem.* **1970**,

2, 225. b) W. L. Dilling, N. B. Tefertiller, A. B. Mitchell, *Mol. Photochem.* **1973**, *5*, 371. c) C. Kaneko, H. Fujii, K. Kato, *Heterocycles* **1982**, *17*, 395. d) N. Katagiri, M. Sato, N. Yoneda, S. Saikawa, T. Sakamoto, M. Muto, C. Kaneko, *J. Chem. Soc., Perkin Trans. 1* **1986**, 1289. e) H. Hongo, K. Iwasa, C. Kabuto, H. Matsuzaki, H. Nakano, *J. Chem. Soc., Perkin Trans. 1* **1997**, 1747. f) S. M. Sieburth, *Photochemical Reactivity of Pyridones*, in *CRC Handbook of Organic Photochemistry and Photobiology*, 2nd ed., ed. by W. Horspool, E. Lenci, CRC Press, **2003**, Chap. 103-1.

33 a) J. L. Broeker, J. E. Eksterowicz, A. J. Belk, K. N. Houk, *J. Am. Chem. Soc.* **1995**, *117*, 1847. b) E. García-Expósito, M. J. Bearpark, R. M. Ortuño, M. A. Robb, V. Branchadell, *J. Org. Chem.* **2002**, *67*, 6070.

34 a) A. Yokoyama, K. Mizuno, *Org. Lett.* **2000**, *2*, 3457. b) K. Matsubayashi, Y. Kubo, *J. Org. Chem.* **2008**, *73*, 4915.

35 T. Shimo, T. Uezono, T. Obata, M. Yasutake, T. Shinmyozu, K. Somekawa, *Tetrahedron* **2002**, *58*, 6111.

36 K. Somekawa, R. Izumi, K. Taniguchi, T. Suishu, S. Tokita, *Nippon Kagaku Kaishi* **1990**, 271.

37 a) E. Fischer, R. Gleiter, *Angew. Chem., Int. Ed. Engl.* **1989**, *28*, 925. b) R. Gleiter, W. Sander, *Angew. Chem., Int. Ed. Engl.* **1985**, *24*, 566. c) R. Srinivasan, K. H. Carlough, *J. Am. Chem. Soc.* **1967**, *89*, 4932.

38 J. D. Xidos, R. A. Poirier, C. C. Pye, D. J. Burnell, *J. Org. Chem.* **1998**, *63*, 105.

39 J. W. Hanifin, E. Cohen, *J. Org. Chem.* **1968**, *33*, 2811.

40 D. J. Haywood, R. G. Hunt, C. J. Potter, S. T. Reid, *J. Chem. Soc., Perkin Trans. 1* **1977**, 2458.

41 T. Naito, N. Nakayama, C. Kaneko, *Chem. Lett.* **1981**, 423.

42 S. Nonoyama, N. Yonezawa, K. Saigo, M. Hasegawa, Y. Iitaka, *Bull. Chem. Soc. Jpn.* **1987**, *60*, 349.

43 M. Yasuda, T. Kishi, C. Goto, H. Satoda, K. Nakabayashi, T. Minami, K. Shima, *Tetrahedron Lett.* **1992**, *33*, 6465.

44 K. Kobayashi, M. Suzuki, H. Suginome, *J. Chem. Soc., Perkin Trans. 1* **1993**, 2837.

45 T. Shimo, K. Date, K. Somekawa, *J. Heterocycl. Chem.* **1992**, *29*, 387.

46 a) S. Sakaki, *Kagaku-Sousetsu*, No. 47, Gakkai Shuppan Center, Tokyo, **2000**, p. 179. b) K. Sameshima, *Computational Chemistry*, in *The Fifth Series of Experimental Chemistry*, Maruzen, Tokyo, **2004**, Vol. 12, p. 48. c) S. Tokita, K. Somekawa, *Ryoshi-Kagaku no Kiso*, Shokabo, Tokyo, **2005**, p. 147. d) H. Sakiyama, A. Kazama, S. Suzuki, Y. Nishida, *J. Comput. Chem. Jpn.* **2008**, *7*, 27.

47 a) M. Nishio, *Tetrahedron* **2005**, *61*, 6923. b) T. Obata, T. Shimo, M. Yasutake, T. Shinmyozu, M. Kawaminami, R. Yoshida, K. Somekawa, *Tetrahedron* **2001**, *57*, 1531.

48 a) H. Nishino, A. Nakamura, Y. Inoue, *J. Chem. Soc., Perkin Trans. 2* **2001**, 1693. b) K. Raghavachari, R. C. Haddon, H. D. Roth, *J. Am. Chem. Soc.* **1983**, *105*, 3110. c) M. Z. Kassaee, E. Vessally, *THEOCHEM* **2005**, *716*, 159. d) A. Tsubata, T. Uchiyama, A. Kameyama, T. Nishikubo, *Macromolecules* **1997**, *30*, 5649.

49 *Hikari-to-Kagaku-no-Jiten*, ed. by Hikari-to-Kagaku-no-Jiten-Henshuiinkai, Maruzen, Tokyo, **2002**, pp. 318–325.

50 S. Minakata, S. Moriwaki, H. Inada, M. Komatsu, H. Kajii, Y. Ohmori, M. Tsumura, K. Namura, *Chem. Lett.* **2007**, *36*, 1014.

51 J. A. Joule, K. Mills, *Heterocyclic Chemistry*, 4th ed., Blackwell Publishing, **2007**, p. 129.

52 M. C. Pirrung, A. B. Bleecker, Y. Inoue, F. I. Rodríguez, N. Sugawara, T. Wada, Y. Zou, B. M. Binder, *Chem. Biol.* **2008**, *15*, 313.

Kenichi Somekawa is Professor Emeritus at Kagoshima University and the part-time Instructor since spring 2007. He was born in Kagoshima, Japan in 1941. After graduating Faculty of Engineering in Kagoshima University, he entered Graduate School of Engineering in the University of Tokyo. After receiving M.Eng. degree from the University of Tokyo, he worked for organic syntheses at Professor S. Kumamoto's group in Kagoshima University from 1966. After receiving Ph.D. degree of engineering under Professor T. Matsuo from Kyushu University (1982), he joined to Professor P. S. Mariano's group at University of Maryland as a postdoc. He was a professor of Kagoshima University from 1984 to 2007. He stayed at Professor Jean-M. Lehn's labo. in the University of Strasbourg five months in 1992. His research interest is mainly photochemistry evolution by molecular simulation by use of MO method.

Tetsuro Shimo is Associate Professor at the Graduate School of Science and Engineering, Kagoshima University since 2009. He received his B.Eng. degree (1971) from Kagoshima University and Ph.D. degree (1988) from Kyushu University. He joined Kagoshima University (Prof. S. Kumamoto's group) as an Assistant Professor in 1973 and was promoted to Associate Professor in 1989. He worked as a postdoctoral fellow with Prof. A. G. Fallis at Ottawa University from 1989. He joined the Faculty of Engineering, Kagoshima University in 1990. He moved to the Institute for Fundamental Research of Organic Chemistry, Kyushu University, as an Associate Professor in 1999 and moved to the Faculty of Engineering, Kagoshima University in 2001.